Mapping the evolution of pure CO2 ices irradiated by ions, UV, and electrons using the upgraded PROCODA code (employing an effective rate constant ordering by thermochemistry data)

Pilling, S.; Monteiro Rocha, W.R.; Carvalho, G.A.; Abreu, H.A. de

Available online at www.sciencedirect.com

ScienceDirect

Advances in Space Research 71 (2023) 5466–5492

ADVANCES IN SPACE RESEARCH (a COSPAR publication)

www.elsevier.com/locate/asr

Mapping the evolution of pure CO_2 ices irradiated by ions, UV, and electrons using the upgraded PROCODA code (employing an effective rate constant ordering by thermochemistry data)

Sergio Pilling [a,*], Will R.M. Rocha [b], Geanderson A. Carvalho [a], Heitor A. de Abreu [c]

[a] Instituto de Pesquisa e Desenvolvimento, Universidade do Vale do Paraíba, São José dos Campos 12244-000, SP, Brazil
[b] Laboratory for Astrophysics, Leiden Observatory, Leiden University, PO Box 9513, NL2300 RA Leiden, the Netherlands
[c] Departamento de química, Universidade Federal de Minas gerais – UFMG, Belo Horizonte 31270-901, MG, Brazil

Received 6 October 2022; received in revised form 11 January 2023; accepted 1 February 2023
Available online 6 February 2023

Abstract

Chemical reactions and desorption processes are being triggered by incoming ionizing radiation over astrophysical ices in cold space environments. The quantification of these processes is crucial to achieve a detailed understanding of the underlying chemistry occurring within the ice. With this goal, we have upgraded the PROCODA code (Pilling et al. 2022a) which solves a system of coupled differential equations and describes the evolution of the molecular abundances under processing by radiation, now including an effective rate constant (ERCs) ordering by employing thermochemistry data taken from literature. This methodology helps to identify the most important reactions within the reaction network and therefore decreases the degeneracy of the solutions and enhancing the accuracy of the calculations. Here, we described the chemical evolution of four irradiated pure CO_2 considering 11 different chemical species, 100 reaction routes and 11 radiation-induced desorption processes. The best-fit models provide the effective rate constants, several desorption parameters, as well as, the characterization of the chemical equilibrium (CE) phase. A comparison with previous code version was given and indicates that the ordering of rate constants by thermochemistry data is more important when more energy is deposited in the ice. The current work present more realistic values for the effective rate constants and a better characterization of the CE phase, such data can be used to refine astrochemical models to better describe cold space environments in the presence of incoming ionizing radiation field such molecular clouds and protoplanetary regions and the surface of comets and frozen moons and planets.

Keywords: ISM: molecules; Astrochemistry; Molecular data; Molecular processes; Software: simulations; Solid state: volatile

1. Introduction

In cold space environments, chemical reactions and desorption processes are being triggered by incoming ionizing radiation impinging astrophysical ices (e.g. Muñoz Caro et al. 2002; Meinert et al. 2016). This radiation-induced processing leads to an increase in chemical complexity in the ices, as well as in their gaseous vicinity (e.g. van Dishoeck 2014; Boogert et al. 2015). Among the chemical inventory in the interstellar medium, carbon dioxide (CO_2), an apolar molecule with linear geometry, is ubiquitously found in the interstellar medium (e.g., de Graauw et al. 1996, Gerakines et al. 1999, Pontoppidan et al. 2008, Poteet et al. 2013, Ehrenfreund & Charnley 2000; Fraser et al. 2002, Öberg et al. 2011) and on icy moons of the solar system (Buratti et al. 2005, Cartwright et al. 2015). The irradiation of pure CO_2 ice by UV radiation has shown that other molecules, such as CO, O_3, and CO_3, can be formed in the ice (Gerakines et al. 1996). Addi-

* Corresponding author.
E-mail address: spilling@univap.br (S. Pilling).

https://doi.org/10.1016/j.asr.2023.02.002
0273-1177/

tionally, other experiments addressing the influence of other energy regimes have also been performed. In particular, Mejía et al. (2015) and Pilling et al. (2010a) studied the impact of cosmic ray analogs on ice chemistry, and chemical processes induced by electrons and UV photons have been addressed by Bennett et al. (2004) and Martín-Doménech et al. (2015), respectively.

The underlying chemistry occurring within the ice when exposed to ionizing radiation is not accessible from experiments. In fact, the in situ techniques used to analyze the ice such as infrared spectroscopy and mass spectrometry work as diagnostic tools to visualize the differences in the ice's chemical composition before and after irradiation. To have insights into the chemistry triggered by radiation a chemical model simulating laboratory conditions is necessary. With this goal, the PROCODA code, which stands for PROgram for solving COupled Differential equations in Astrochemistry, was developed (Pilling et al. 2022a). It solves a system of coupled differential equations and describes the evolution of the molecular abundances of ices under processing by radiation. This methodology is complementary to other attempts to understand chemical reactions in the ice carried out, for example, by Jamieson et al. (2006), Bossa et al. (2015), Shingledecker et al. (2019) and Rocha et al. (2022). Additionally, the code calculates the effective rate constants (ERCs) of the direct, bimolecular and termolecular reactions, the radiation-induced desorption effective rate constants, as well as the desorption column density for the studied species as functions of time and the summed molecular desorption yield (Y). It is worth noting that the direct reactions mean the dissociation or destruction reactions triggered by the incoming radiation (which might also involve the action of secondary electrons). A discussion on the role of secondary electrons can be found at Mason et al. (2014) and Boyer et al. (2016).

The PROCODA code also provides abundances for both observed and non-observed (unknown) species in the IR spectra during ice chemical evolution during processing by incoming radiation, and also characterizes the chemical equilibrium (CE) phase in the ice that occurs at larger radiation fluence. Recently, the PROCODA code has been employed to map the CE phase of pure acetonitrile (CH_3-CN) and carbon monoxide (CO) ices exposed to ionizing radiation (Carvalho et al. 2022; Pilling et al. 2022b).

The current modifications in the code (the ERCs ordering hypothesis by thermochemistry data) help to identify the most important reactions within the reaction network and therefore decrease the degeneracy of the solutions and enhance the accuracy of the calculations. With the upgraded PROCODA code we map the chemical evolution of four pure CO_2 ices exposed to different ionizing radiation sources (52 MeV $^{58}Ni^{+13}$ ions, 550 MeV $^{50}Ti^{+21}$ ions, 10 eV photons, 5 keV electrons). An extended comparison between the current code version with the previous version also applied to CO_2 ices (without ordering hypothesis) described by Pilling et al. (2022a) for two models (Ni ions and UV photons) was given, and the main changes and similarities were discussed. In a few words, the upgraded code version allows a decrease in the solution's degeneracy and also allows a better accuracy for the calculated rates constants, desorption yields, and molecular abundances.

It is worth noting that the current methodology highlights the employ of the term "effective" rate constant (ERC), which is a parameter with a broader concept than the "ordinary" rate constant (k) of reaction, commonly considered in gas phase chemistry. The ERCs handle the fact that reactants within the ice are surrounded by different neighbors, which also vary with time (and also are affected by the grain's local density and temperature due to the incoming radiation). Therefore, this quantity, in some sense, represents an average value (in time and space) over the ice during this ice processing by radiation and better describes what is happening within the ice in real conditions. To provide more realistic results, the astrochemical ice models should consider this ERC instead of an "ordinary" rate constant for a given reaction (often employed the gas-phase values also for ices) since the ice composition is not strictly homogeneous and also varies with time, and are also under radiation processing.

The computational methodology in this work, which includes the hypothesis of ordering of rate constant by employing thermochemistry data and the details of the employed experimental works, is described in section 2. The results employing the upgraded PROCODA code in four pure CO_2 ices exposed to ionizing radiation are shown in Section 3, presenting also the characterization of the CE phase, as well as a comparison with the previous version of the code. Some astrophysical implications are provided in section 4. Section 5 lists the main conclusions and presents final remarks.

2. Methodology

In the current work, we present the upgraded version of the PROCODA code (the original code is given by Pilling et al. 2022a) which solves a system of coupled differential equations to describe the chemical evolution, as a function of time, of typical astrophysical ices during processing by ionizing radiation. The current version considers an ordering hypothesis for the effective rate constants (ERCs) by employing thermochemistry data (gas-phase at 0 K). In the manuscript, we prefer to use the term "effective" to describe the rate constants, making explicit that this physicochemical parameter takes into account the different chemical environments in which a given reaction may occur within the ice (an average value). Details on this ordering hypothesis will be provided further.

It is worth noting that, in this manuscript, we sometimes present the ERCs as k values (e.g., k1, k2, k_{des}, k_{A+B}).

2.1. Experimental datasets

The employed chemical network considers 100 coupled equations that describe the chemical evolution of selected

molecules formed from pure CO_2 ices under the presence of different types of ionizing radiation. The reaction set also takes radiation-induced molecular desorption into account. The proposed reaction network involves 11 molecular species (the parent species CO_2 and the newly produced species CO, O_3, CO_3, O, O_2, C, C_2, C_2O, C_2O_2, and C_2O_3). Fig. 1 illustrates the Lewis structures of the species involved in the CO_2 ice decomposition process. These species were chosen since they present the lowest formation enthalpy energies.

Here, four experimental datasets were considered employing different ionizing sources on pure CO_2 ice: i) 15 K ice bombarded by 550 MeV $^{50}Ti^{+21}$ ions (from Mejía et al. 2015) named as CR1 model; ii) 13 K ice bombarded by 52 MeV $^{58}Ni^{+13}$ ions (from Pilling et al. 2010a) named as CR2 model; iii) 10 K ice bombarded by 5 keV electrons (from Bennett et al. 2004) named as EL model; and iv) 8 K ice irradiated by UV photons of ~ 10 eV (from Martín-Doménech et al. 2015) named as UV model. Following the authors, the experimental uncertainties were below 10–20 %. It is worth noting that, in all cases, only the four observable species (CO_2, CO, O_3, and CO_3) were quantified in the experimental data. With the current methodology, we can map and characterize the abundances of the other seven proposed non-observable species (O, O_2, C, C_2, C_2O, C_2O_2, and C_2O_3), expected to have formed during the irradiated CO_2 ice experiments.

2.2. The PROCODA methodology

As discussed by Pilling et al. (2022a) the typical equation in the chemical coupled system solved by PROCODA code has the following parameters:

$$\frac{dN_i}{dt} = \left[-DES_i(t) - \sum_{d1} k_{d1}N_i(t) - \sum_{d2} k_{d2}N_i(t)N_a(t) - \sum_{d3} k_{d3}N_i(t)N_a(t)N_b(t)\right] + \left[\sum_{p1} k_{p1}N_a(t) + \sum_{d2} k_{p2}N_a(t)N_b(t) + \sum_{p3} k_{p3}N_a(t)N_b(t)N_c(t)\right] \left[\text{molecules cm}^{-2}\,\text{s}^{-1}\right] \quad (1)$$

where dN_i/dt is the column density changes of a given molecule i along the time t, the k values are the ERCs for different processes, and $DES_i(t) = k_{des,i}\Omega_i(t)N_i(t)$ is the differential column density desorption, i.e., the number of molecules (or atomic species) that desorbs from ice to gas-phase per cm^2 and per second due to incoming radiation which depends also on the intrinsic radiation-induced desorption rate constant ($k_{des,i}$), in units of s^{-1}, the and the dimensionless surface coverage of the species i as a function of time ($\Omega_i(t)$). The desorption itself was considered a first-order type reaction. In this equation, the values k_{d1}, k_{d2}, and k_{d3} represent the destruction processes (consumption) and the values k_{p1}, k_{p2}, and k_{p3} represent the production processes (formation) of a given species in direct, bimolecular, and termolecular reactions, respectively (details are given at Pilling et al. 2022a). The values N_a, N_b, and N_c indicate the concentrations of species a, b and c, respectively, which participate in in the reaction to produce or consume the respective i species.

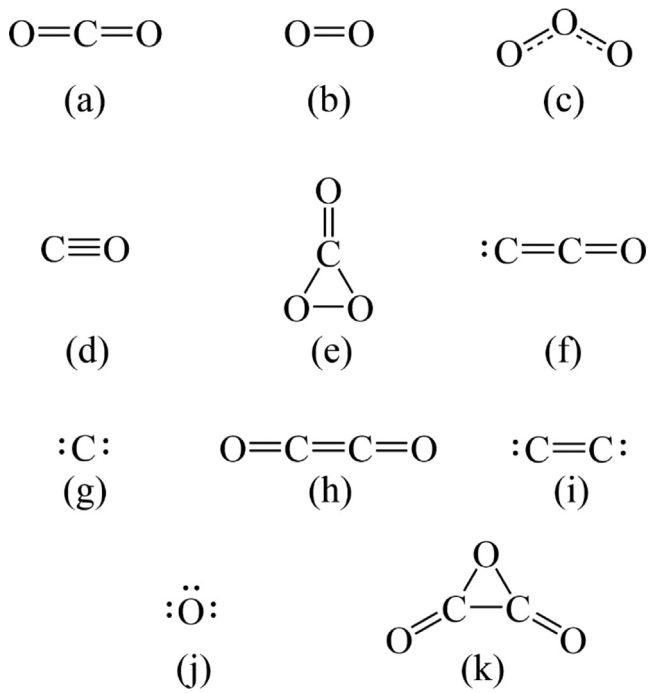

Fig. 1. Lewis structures of the eleven species formed in the CO_2 ice decomposition process. (a) CO_2, (b) O_2, (c) O_3, (d) CO, (e) CO_3, (f) C_2O, (g) C, (h) C_2O_2, (i) C_2, (j) O, (k) C_2O_3.

It is worth noting that the code applies other constraints besides the minimization of chi-square function for the data, such as, mass conservation, desorption yield and CE phase. Those constraints are employed in a minimization process of a function (named score function (SF)) that evaluates how close the system is to its minimum global solution. The score function is defined as follows

$$\begin{aligned} SF = {} & p1 \times \sum \frac{(oCO2_{data} - oCO2_{model})^2}{oCO2_{data}} + \\ & p2 \times \sum \frac{(oCO_{data} - oCO_{data})^2}{oCO_{data}} + \\ & p3 \times \sum \frac{(oO3_{data} - oO3_{model})^2}{oO3_{data}} + \\ & p4 \times \sum \frac{(oCO3_{data} - oCO3_{model})^2}{oCO3_{data}} + \\ & p5 \times [(1 - \text{MSC}_\text{f}) + (1 - \text{MSCo}_\text{f}) + (1 - \text{MSCo}_\text{m})] + \\ & p6 \times (1 - \text{DSC}) + p7 \times (1 - \text{SSC}) \end{aligned} \quad (2)$$

where the dimensionless parameters $p1$ to $p7$ in this equation are the weights of each term, used as a tool to search for the best solution during the computational minimization processes. In this equation, the parameter MSC_f is the model mass similarity criterion (or model mass conservation), calculated considering the similarity between the initial column mass of the modeled system and the total column mass of the model at final modeling time (at largest time) (including both masses, at the ice and desorbed), $MSCo_f$ and $MSCo_m$ are the column mass similarity criterion between the experimentally observed column mass and the observed column mass in the model at the final

modeling time and at the middle of the modeling time, respectively. From these three parameters, we calculate a parameter called mass similarity criterion $MSC = (MSC_f \times 100\,\% + MSCo_f \times 100\,\% + MSCo_m \times 100\,\%)/3$, which also helps to indicate how good is the solution of the system in compared with the observed data. The parameter *DSC* is the desorption similarity criterion, calculated considering the similarity of the input expected desorption yield (based on the manuscripts with the experimental data employed) and the total molecular desorption yield computed by the model. The parameter *SSC* is the slope similarity criterion, which is related to the achievement of CE phase in the ice at larger radiation fluence, as described in Pilling et al. (2022a).

It is worth noting that the chi-squared function χ^2 (also named summed CHI2) can be obtained directly from equation [2] making $p1 = p2 = p3 = p4 = 1$ and $p5 = p6 = p7 = 0$. The chi-squared function is a parameter obtained considering the experimental concentration data of the observed molecules (CO_2, CO, O_3, and CO_3) and their modeled concentration.

For each model, the code was typically run three times until the best-fit solution was found. At every new run, the obtained ERCs in the previous best-fit calculations were considered as new input for the new calculations. The details of the code, including the employed equations, the coupled equation minimization algorithm (L_BFGS-B algorithm), its explanatory flowchart, the input and output parameters, and the criteria for model convergence can be found at Pilling et al. (2022a).

2.3. The ordering hypothesis for the effective rate constants (code upgrade)

In this upgraded version of the code, we consider, as a first approximation, that in a given set of reactions (with the same initial reactants), the ones with smaller enthalpy variation, ΔH (more exothermic), are expected to have a larger rate constant, k (faster reactions). This hypothesis is also supported by the Evans–Polanyi principle (also referred to as the Bell-Evans-Polanyi principle) which observes that the difference in activation energy between two reactions of the same family is proportional to the difference in their enthalpy of reaction (Bell 1936; Evans and Polanyi, 1936). The Evans-Polanyi model is a linear energy relationship that serves as an efficient way to calculate the activation energy of many reactions within a distinct family. The activation energy may be used to characterize the kinetic rate parameter of a given reaction through the application of the Arrhenius equation.

As a first approximation, the thermochemical data used in the ordering hypothesis for the ERCs, considers that all studied species are in the lowest energy level and formation enthalpies and reaction enthalpies are at gas-phase at the theoretical temperature of 0 K. It is worth noting that the hypothesis of the ordering of ERCs was implemented only for the reactions within the reaction groups. In this manuscript, we have considered a total of 28 reaction groups (each one containing different reaction pathways or different routes inside) in the code, named from G1 to G28. Each group has its own ordering in the rate constants, and this ordering is independent of the ordering in other groups. Single reactions (the ones that do not belong to a specific reaction group) were not ranked by thermochemistry data. The rate constant ordering was introduced in the code by adding boundary constraints in the calculation of each rate of reaction inside a specific reaction group.

The values of reaction enthalpies considered in this work and the ordering of rate constants within the different reaction groups are indicated in the Table 2. For the reactions involving the species CO_2, CO, O, O_2, O_3, C, C_2, C_2O, C_2O_2 it was employed the gas-phase 0 K formation enthalpies values $\Delta_fH(CO_2) = -393.1$ kJ mol^{-1}; $\Delta_fH(CO) = -113.8$ kJ mol^{-1}; $\Delta_fH(O_3) = 144.3$ kJ mol^{-1}; $\Delta_fH(O) = 246.8$ kJ mol^{-1}; $\Delta_fH(O_2) = 0$ kJ mol^{-1}; $\Delta_fH(C) = 711.4$ kJ mol^{-1}; $\Delta_fH(C_2) = 820.2$ kJ mol^{-1}; $\Delta_fH(C_2O) = 337.1$ kJ mol^{-1}; $\Delta_fH(C_2O_2) = 14$ kJ mol^{-1}, obtained from the Active Thermochemical Tables version 1.122p at https://atct.anl.gov/ (see also Ruscic et al. 2004; Ruscic et al. 2005; Ruscic & Bross 2020). For the reactions involving CO_3, it was assumed the gas-phase formation enthalpies at 0 K of $\Delta_fH = 52.5$ kJ mol^{-1}, and the reactions enthalpies Δ_rH were obtained from the NIST website (https://cccbdb.nist.gov/). For the reactions involving C_2O_3 it was considered the 0 K formation enthalpies $\Delta_fH(C_2O_3) = -282.2$ kJ mol^{-1} (from Gambi et al. (2001) together with the other formation enthalpies from ATCL at https://atct.anl.gov/). It is worth noting that some reactions considered in the model (see Table 2) are endothermic (at gas-phase) and might be difficult to occur in the ice at low temperatures, however since the suited ices are constantly under bombardment (with constant energy input by the incoming projectiles) such reactions may have indeed a chance to occur.

2.4. Limitations and advantages of the code

It is worth noting that, the current model does not consider, in an explicit way, the ionic and excited (thermally, electronically, or vibrationally states) species. However, we understand that such chemical states should belong to the reactions inventory within the ice. The ERC calculated here, for example, in the reaction $A + RAD \rightarrow B + C$ (where $RAD =$ any type of radiation) in some way involves the different chemical states in which A, B, or C species appear in the ice (which includes neutral, ionic, excited and radical). The major difficulty in considering these forms separately in the models is not in writing the coupled equations, but in the way to measure them in the experimental data at IR. Future work will include explicitly introducing a few ionic species to the model (considering as one of the working hypotheses, for example, a specific ratio ion/neutral for a selected species in the ice).

Table 1
The considered reaction routes and the calculated effective rate constants (ERC) employing the upgraded PROCODA code on pure CO_2 irradiated ices. The reaction enthalpies considered in the ordering hypothesis for the ERC and the reaction groups (with the ordering of ERCs between parentheses) are listed. The intrinsic values for molecular desorption are listed at the bottom at the table.

Modelled reactions[a]	Effective rate constant (CR1 / CR2 / EL / UV)	Reaction enthalpy at 0 K[b] [kJ/mol]	Reaction groups (*k* values ordered based on reaction exothermicity) [c]	References or comments
$CO_2 + RAD \rightarrow CO + O$	k1 = (3.1e-06 / 9.4e-07 / 1.6e-06 / 1.3e-08) s^{-1}	526.1	G1 (k1 > k3 > k5)	[3,4,5,6] gas-phase; [9,10] ice
$CO + O \rightarrow CO_2$	k2 = (3.1e-27 / 2.4e-26 / 1.4e-24 / 2.9e-26) cm^3 $molecule^{-1}$ s^{-1}	−526.1	G8 (k2 > k69)	[3] gas and surface; [4] gas-phase
$CO_2 + RAD \rightarrow C + O_2$	k3 = (1.6e-8/<1.0e-08 / 1.2e-08 / <7.6e-09) s^{-1}	1104.5	G1 (k1 > k3 > k5)	[12] ice; [13] Desorption,
$C + O_2 \rightarrow CO_2$	k4 = (5.3e-26 / 2.5e-25 / 3.2e-25 / 5.8e-27) cm^3 $molecule^{-1}$ s^{-1}	−1104.5	G9 (k4 > k70)	[3] gas and surface; [4] gas-phase
$CO_2 + RAD \rightarrow C + O + O$	k5 = (≤1.0e-08 / ≤ 1.0e-08 / ≤ 1.0e-08 / ≤ 1.0e-08) s^{-1}	1598.2	G1 (k1 > k3 > k5)	
$C + O + O \rightarrow CO_2$	k6 = (1.2e-48 / 3.4e-48 / 2.2e-48 / 1.1e-49) cm^6 $molecule^{-2}$ s^{-1}	−1598.2	Single reaction pathway	
$CO_2 + CO_2 \rightarrow C_2O_2 + O_2$	k7 = (8.4e-31 / 4.4e-31 / 4.0e-31 / 4.1e-31) cm^3 $molecule^{-1}$ s^{-1}	800.3	G2 (k13 > k9 > *k*11 > k7)	
$C_2O_2 + O_2 \rightarrow CO_2 + CO_2$	k8 = (4.5e-27 / 4.6e-25 / 1.9e-26 / 6.1e-26) cm^3 $molecule^{-1}$ s^{-1}	−800.3	Single reaction pathway	
$CO_2 + CO_2 \rightarrow CO + CO + O_2$	k9 = (1.0e-30 / 2.4e-28 / 1.5e-28 / 8.0e-28) cm^3 $molecule^{-1}$ s^{-1}	558.6	G2 (k13 > k9 > *k*11 > k7)	
$CO + CO + O_2 \rightarrow CO_2 + CO_2$	*k*10 = (7.0e-49 / 1.2e-47 / 5.1e-48 / 1.5e-48) cm^6 $molecule^{-2}$ s^{-1}	−558.6	Single reaction pathway	
$CO_2 + CO_2 \rightarrow C_2O_3 + O$	*k*11 = (1.1e-30 / 4.2e-31 / 4.8e-31 / 3.0e-31) cm^3 $molecule^{-1}$ s^{-1}	750.8	G2 (k13 > k9 > *k*11 > k7)	Employing $\Delta_f H(C_2O_3)$ = -282.2 kJ mol-1 from Gambi et al. 2001
$C_2O_3 + O \rightarrow CO_2 + CO_2$	k12 = (3.0e-27 / 3.6e-25 / 4.0e-30 / 2.8e-25) cm^3 $molecule^{-1}$ s^{-1}	−750.8	Single reaction pathway	Employing $\Delta_f H(C_2O_3)$ = -282.2 kJ mol-1 from Gambi et al. 2001
$CO_2 + CO_2 \rightarrow CO_3 + CO$	k13 = (3.7e-29 / 1.9e-27 / 1.2e-28 / 1.5e-26) cm^3 $molecule^{-1}$ s^{-1}	503.7	G2 (k13 > k9 > *k*11 > k7)	Employing $\Delta_r H$ from https://cccbdb.nist.gov/
$CO_3 + CO \rightarrow CO_2 + CO_2$	k14 = (2.3e-27 / 2.2e-25 / 3.4e-25 / 5.4e-25) cm^3 $molecule^{-1}$ s^{-1}	−503.7	Single reaction pathway	Employing $\Delta_r H$ from https://cccbdb.nist.gov/
$CO_2 + O \rightarrow CO + O_2$	k15 = (5.3e-28 / 1.1e-26 / 3.0e-26 / 8.0e-26) cm^3 $molecule^{-1}$ s^{-1}	32.4	G3 (k15 > k19 > k17)	[3,5] gas-phase
$CO + O_2 \rightarrow CO_2 + O$	k16 = (1.9e-26 / 1.7e-25 / 2.0e-25 / 1.5e-26) cm^3 $molecule^{-1}$ s^{-1}	–32.4	G19 (k77 > k16 > k75)	[3,4] gas-phase
$CO_2 + O \rightarrow C + O_3$	k17 = (2.4e-28 / 4.4e-31 / 4.9e-28 / 1.4e-26) cm^3 $molecule^{-1}$ s^{-1}	1002.0	G3 (k15 > k19 > k17)	
$C + O_3 \rightarrow CO_2 + O$	k18 = (2.4e-26 / 4.7e-25 / 3.9e-25 / 1.9e-25) cm^3 $molecule^{-1}$ s^{-1}	−1002.0	G22 (k18 > k76)	
$CO_2 + O \rightarrow CO_3$	k19 = (1.1e-29 / 9.0e-27 / 3.0e-27 / 3.1e-26) cm^3 $molecule^{-1}$ s^{-1}	52.5	G3 (k15 > k19 > k17)	[5] gas-phase; [10] ice; Employing enthalpies from https://cccbdb.nist.gov/
$CO_3 + RAD \rightarrow CO_2 + O$	k20 = (2.6e-04 / 1.8e-02 / 2.0e-03 / ≤ 9.0e-09) s^{-1}	−52.5	G12 (k20 > k78 > k87)	[5] gas-phase; [10] ice; Employing enthalpies from https://cccbdb.nist.gov/
$CO_2 + O_2 \rightarrow CO + O_3$	k21 = (1.2e-26 / 7.7e-25 / 1.1e-24 / 2.5e-26) cm^3 $molecule^{-1}$ s^{-1}	423.7	G4 (k21 > k25 > k23)	
$CO + O_3 \rightarrow CO_2 + O_2$	k22 = (1.1e-26 / 9.9e-26 / 2.9e-25 / 4.8e-26) cm^3 $molecule^{-1}$ s^{-1}	− 423.7	G10 (k22 > k79)	
$CO_2 + O_2 \rightarrow C + O + O_3$	k23 = (2.4e-27 / 1.1e-28 / 1.3e-26 / 1.7e-29) cm^3 $molecule^{-1}$ s^{-1}	1495.7	G4 (k21 > k25 > k23)	
$C + O + O_3 \rightarrow CO_2 + O_2$	k24 = (4.8e-49 / 1.6e-48 / 5.3e-48 / 2.4e-49) cm^6 $molecule^{-2}$ s^{-1}	−1495.7	Single reaction pathway	
$CO_2 + O_2 \rightarrow CO_3 + O$	k25 = (4.8e-27 / 3.1e-26 / 1.5e-25 / 4.7e-27) cm^3 $molecule^{-1}$ s^{-1}	445.6	G4 (k21 > k25 > k23)	Employing enthalpies from https://cccbdb.nist.gov/
$CO_3 + O \rightarrow CO_2 + O_2$	k26 = (5.3e-26 / 4.7e-24 / 7.1e-26 / 2.8e-25) cm^3 $molecule^{-1}$ s^{-1}	−445.6	G28 (k26 > k80)	
$CO_2 + C \rightarrow C_2 + O_2$	k27 = (8.4e-31 / 4.8e-27 / 6.8e-29 / 2.2e-26) cm^3 $molecule^{-1}$ s^{-1}	501.9	G5 (k29 > k31 > k27)	
$C_2 + O_2 \rightarrow CO_2 + C$	k28 = (5.0e-27 / 8.5e-26 / 8.3e-27 / 6.2e-25) cm^3 $molecule^{-1}$ s^{-1}	−501.9	G24 (k62 > k28)	[3] gas-phase
$CO_2 + C \rightarrow CO + CO$	k29 = (1.1e-26 / 1.3e-25 / 2.0e-25 / 1.4e-25) cm^3 $molecule^{-1}$ s^{-1}	−545.8	G5 (k29 > k31 > k27)	[3,4] gas-phase
$CO + CO \rightarrow CO_2 + C$	k30 = (1.2e-26 / 1.7e-26 / 2.4e-25 / 9.1e-28) cm^3 $molecule^{-1}$ s^{-1}	545.8	G11(k59 > k30 > k63 > k61)	[7,8] ice
$CO_2 + C \rightarrow C_2O_2$	k31 = (4.4e-27 / 6.3e-26 / 1.4e-26 / 1.2e-25) cm^3 $molecule^{-1}$ s^{-1}	−304.3	G5 (k29 > k31 > k27)	

Table 1 (*continued*)

Modelled reactions[a]	Effective rate constant (CR1 / CR2 / EL / UV)	Reaction enthalpy at 0 K[b] [kJ/mol]	Reaction groups (*k* values ordered based on reaction exothermicity) [c]	References or comments
$C_2O_2 + RAD \rightarrow CO_2 + C$	k32 = (2.4e-03 / 2.5e-03 / 3.7e-03 / 5.4e-03) s^{-1}	304.3	G15 (k60 > k32 > k93)	
$CO_2 + CO \rightarrow C_2O_3$	k33 = (1.6e-28 / 4.3e-27 / 2.9e-28 / 1.6e-27) cm^3 $molecule^{-1}$ s^{-1}	224.7	G6 (k33 > k35 > k37 > k39)	Employing $\Delta_fH(C_2O_3)$ = -282.2 kJ mol-1 from Gambi et al. 2001
$C_2O_3 + RAD \rightarrow CO_2 + CO$	k34 = (1.7e-04 / 5.3e-02 / 3.1e-03 / 5.0e-03) s^{-1}	−224.7	G16 (k34 > k95 > k97 > k99)	Employing $\Delta_fH(C_2O_3)$ = -282.2 kJ mol-1 from Gambi et al. 2001
$CO_2 + CO \rightarrow C_2O_2 + O$	k35 = (6.6e-29 / 4.5e-28 / 4.5e-29 / 3.9e-28) cm^3 $molecule^{-1}$ s^{-1}	767.8	G6 (k33 > k35 > k37 > k39)	
$C_2O_2 + O \rightarrow CO_2 + CO$	k36 = (1.7e-25 / 2.4e-25 / 3.0e-26 / 2.8e-25) cm^3 $molecule^{-1}$ s^{-1}	−767.8	G17 (k36 > k98)	
$CO_2 + CO \rightarrow C_2O + O_2$	k37 = (8.2e-29 / 2.3e-30 / 2.8e-31 / 1.4e-30) cm^3 $molecule^{-1}$ s^{-1}	884.0	G6 (k33 > k35 > k37 > k39)	
$C_2O + O_2 \rightarrow CO_2 + CO$	k38 = (2.0e-26 / 4.4e-25 / 2.1e-26 / 7.7e-25) cm^3 $molecule^{-1}$ s^{-1}	−884.0	G20 (k38 > k100)	
$CO_2 + CO \rightarrow C_2 + O_3$	k39 = (2.3e-28 / 4.4e-31 / 4.0e-31 / 3.4e-27) cm^3 $molecule^{-1}$ s^{-1}	1471.6	G6 (k33 > k35 > k37 > k39)	
$C_2 + O_3 \rightarrow CO_2 + CO$	k40 = (5.4e-27 / 1.8e-25 / 1.5e-25 / 4.4e-26) cm^3 $molecule^{-1}$ s^{-1}	−1471.6	Single reaction pathway	
$CO_2 + C_2O \rightarrow C_2O_2 + CO$	k41 = (2.7e-27 / 1.3e-25 / 4.4e-26 / 8.6e-26) cm^3 $molecule^{-1}$ s^{-1}	−83.0	G21 (k41 > k43)	
$C_2O_2 + CO \rightarrow CO_2 + C_2O$	k42= (7.9e-27 / 5.2e-26 / 2.4e-26 / 3.7e-26) cm^3 $molecule^{-1}$ s^{-1}	83.0	Single reaction pathway	
$CO_2 + C_2O \rightarrow C_2O_3 + C$	k43 = (1.1e-27 / 6.9e-26 / 1.6e-27 / 4.0e-26) cm^3 $molecule^{-1}$ s^{-1}	413,2	G21 (k41 > k43)	Employing $\Delta_fH(C_2O_3)$ = -282.2 kJ mol^{-1} from Gambi et al. 2001
$C_2O_3 + C \rightarrow CO_2 + C_2O$	k44 = (1.0e-26 / 3.3e-25 / 2.6e-27 / 4.4e-26) cm^3 $molecule^{-1}$ s^{-1}	−413,2	Single reaction pathway	Employing $\Delta_fH(C_2O_3)$ = -282.2 kJ mol^{-1} from Gambi et al. 2001
$CO_2 + C_2 \rightarrow CO + C_2O$	k45 = (2.2e-26 / 3.4e-26 / 1.4e-25 / 1.8e-26) cm^3 $molecule^{-1}$ s^{-1}	− 163.90	G25 (k45 > k47)	
$CO + C_2O \rightarrow CO_2 + C_2$	k46 = (1.1e-26 / 1.1e-25 / 1.8e-26 / 1.4e-25) cm^3 $molecule^{-1}$ s^{-1}	163.90	G18 (k46 > k73)	
$CO_2 + C_2 \rightarrow C_2O_2 + C$	k47 = (1.8e-27 / 2.0e-26 / 1.4e-25 / 1.6e-26) cm^3 $molecule^{-1}$ s^{-1}	299.0	G25 (k45 > k47)	
$C_2O_2 + C \rightarrow CO_2 + C_2$	k48 = (2.7e-27 / 1.9e-25 / 2.8e-27 / 2.4e-26) cm^3 $molecule^{-1}$ s^{-1}	−299.0	G27 (k74 > k48)	
$CO_2 + CO_3 \rightarrow C_2O + 2\ O_2$	k49 = (1.5e-27 / 2.3e-25 / 4.6e-28 / 4.1e-31) cm^3 $molecule^{-1}$ s^{-1}	858.87	G7 (k51 > k49)	Employing Δ_rH from https://cccbdb.nist.gov/
$C_2O + 2\ O_2 \rightarrow CO_3 + CO_2$	k50 = (6.2e-49 / 5.1e-47 / 6.9e-50 / 1.1e-48) cm^6 $molecule^{-2}$ s^{-1}	−858.87	Single reaction pathway	Employing Δ_rH from https://cccbdb.nist.gov/
$CO_2 + CO_3 \rightarrow CO + CO + O_3$	k51 = (1.5e-27 / 1.2e-24 / 1.5e-26 / 6.3e-26) cm^3 $molecule^{-1}$ s^{-1}	490.08	G7 (k51 > k49)	Employing Δ_rH from https://cccbdb.nist.gov/
$CO + CO + O_3 \rightarrow CO_3 + CO_2$	k52 = (2.1e-50 / 1.0e-47 / 9.3e-48 / 6.3e-49) cm^6 $molecule^{-2}$ s^{-1}	−490.08	Single reaction pathway	Employing Δ_rH from https://cccbdb.nist.gov/
$CO_2 + O_3 \rightarrow CO + O_2 + O_2$	k53 = (8.4e-31 / 9.8e-29 / 4.9e-29 / 2.4e-27) cm^3 $molecule^{-1}$ s^{-1}	134.9	G23 (k55 > k53)	
$CO + O_2 + O_2 \rightarrow CO_2 + O_3$	k54 = (1.5e-48 / 6.0e-48 / 4.7e-49 / 3.4e-49) cm^6 $molecule^{-2}$ s^{-1}	−134.9	Single reaction pathway	
$CO_2 + O_3 \rightarrow CO_3 + O_2$	k55 = (1.2e-30 / 5.1e-27 / 2.0e-27 / 1.8e-26) cm^3 $molecule^{-1}$ s^{-1}	19.05	G23(k55 > k53)	Employing Δ_rH from https://cccbdb.nist.gov/
$CO_3 + O_2 \rightarrow CO_2 + O_3$	k56 = (1.9e-26 / 7.9e-25 / 2.6e-26 / 3.1e-26) cm^3 $molecule^{-1}$ s^{-1}	−19.05	Single reaction pathway	Employing Δ_rH from https://cccbdb.nist.gov/
$CO + RAD \rightarrow C + O$	k57 = (3.5e-06 / 1.0e-08 / 7.5e-08 / <1.0e-08) s^{-1}	1072.05	Single reaction pathway	[3, 5] gas-phase
$C + O \rightarrow CO$	k58 = (2.6e-26 / 7.7e-26 / 2.1e-24 / 1.1e-25) cm^3 $molecule^{-1}$ s^{-1}	−1072.05	Single reaction pathway	[3] surface [11] ice and desorption
$CO + CO \rightarrow C_2O_2$	k59 = (1.2e-26 / 5.2e-26 / 2.4e-25 / 1.3e-26) cm^3 $molecule^{-1}$ s^{-1}	241.6	G11 (k59 > k30 > k63 > k61)	
$C_2O_2 + RAD \rightarrow CO + CO$	k60 = (9.1e-03 / 5.6e-03 / 2.0e-02 / 1.1e-02) s^{-1}	−241,6	G15 (k60 > k32 > k93)	
$CO + CO \rightarrow C_2 + O_2$	k61 = (8.4e-31 / 1.0e-29 / 1.1e-28 / 4.1e-31) cm^3 $molecule^{-1}$ s^{-1}	1047.9	G11 (k59 > k30 > k63 > k61)	
$C_2 + O_2 \rightarrow CO + CO$	k62 = (1.2e-26 / 8.8e-26 / 1.7e-26 / 6.2e-25) cm^3 $molecule^{-1}$ s^{-1}	−1047.9	G24 (k62 > k28)	[4] gas-phase
$CO + CO \rightarrow C_2O + O$	k63 = (1.5e-28 / 7.7e-28 / 2.1e-27 / 2.8e-31) cm^3 $molecule^{-1}$ s^{-1}	851.6	G11 (k59 > k30 > k63 > k61)	
$C_2O + O \rightarrow 2\ CO$	k64 = (2.3e-26 / 4.3e-26 / 4.0e-26 / 4.0e-25) cm^3 $molecule^{-1}$ s^{-1}	− 851.6	Single reaction pathway	[3,5] gas-phase

(*continued on next page*)

Table 1 (*continued*)

Modelled reactions[a]	Effective rate constant (CR1 / CR2 / EL / UV)	Reaction enthalpy at 0 K[b] [kJ/mol]	Reaction groups (*k* values ordered based on reaction exothermicity) [c]	References or comments
$CO + C \rightarrow C_2O$	k65 = (1.7e-27 / 3.7e-25 / 6.6e-28 / 1.9e-25) cm^3 $molecule^{-1}$ s^{-1}	−220.47	G26 (k65 > k67)	[5] gas-phase; [8] ice
$C_2O + RAD \rightarrow CO + C$	k66 = (2.3e-04 / 2.8e-03 / 1.8e-03 / 9.9e-04) s^{-1}	220.47	G14 (k66 > k91)	[3, 4] gas-phase
$CO + C \rightarrow C_2 + O$	k67 = (1.1e-28 / 3.4e-25 / 4.1e-28 / 5.2e-26) cm^3 $molecule^{-1}$ s^{-1}	469.58	G26 (k66 > k67)	
$C_2 + O \rightarrow CO + C$	k68 = (4.7e-27 / 5.3e-26 / 7.6e-27 / 1.1e-25) cm^3 $molecule^{-1}$ s^{-1}	−469.58	Single reaction pathway	[5] gas-phase
$CO + O \rightarrow C + O_2$	k69 = (8.4e-31 / 1.8e-28 / 4.5e-27 / 2.4e-28) cm^3 $molecule^{-1}$ s^{-1}	578.3	G8 (k2 > k69)	
$C + O_2 \rightarrow CO + O$	k70 = (2.0e-26 / 9.9e-26 / 2.9e-25 / 1.1e-27) cm^3 $molecule^{-1}$ s^{-1}	−578.3	G9 (k4 > k70)	[3] surface; [5,3] gas-phase [11] ice and desorption
$CO + C_2 \rightarrow C_2O + C$	k71= (1.3e-27 / 2.5e-26 / 1.1e-27 / 1.6e-26) cm^3 $molecule^{-1}$ s^{-1}	381.9	Single reaction pathway	
$C_2O + C \rightarrow CO + C_2$	k72 = (1.1e-27 / 9.6e-25 / 4.7e-26 / 1.3e-26) cm^3 $molecule^{-1}$ s^{-1}	−381.9	Single reaction pathway	[3] gas-phase
$CO + C_2O \rightarrow C_2O_2 + C$	K73 = (4.7e-27 / 4.8e-26 / 3.9e-28 / 1.6e-26) cm^3 $molecule^{-1}$ s^{-1}	462.9	G18(k46 > k73)	
$C_2O_2 + C \rightarrow CO + C_2O$	K74 = (2.1e-26 / 2.6e-25 / 1.4e-26 / 3.5e-26) cm^3 $molecule^{-1}$ s^{-1}	−462.9	G27 (k74 > k48)	
$CO + O_2 \rightarrow C + O_3$	K75= (5.9e-27 / 4.6e-26 / 7.9e-26 / 8.4e-27) cm^3 $molecule^{-1}$ s^{-1}	969.59	G19 (k77 > k16 > k75)	
$C + O_3 \rightarrow CO + O_2$	K76 = (7.6e-28 / 1.1e-25 / 6.9e-26 / 1.9e-25) cm^3 $molecule^{-1}$ s^{-1}	−969.59	G22 (k18 > k76)	Employing $\Delta_r H$ from https://cccbdb.nist.gov/
$CO + O_2 \rightarrow CO_3$	K77= (1.9e-26 / 4.3e-25 / 5.9e-25 / 1.1e-26) cm^3 $molecule^{-1}$ s^{-1}	−56.50	G19 (k77 > k16 > k75)	Employing $\Delta_r H$ from https://cccbdb.nist.gov/
$CO_3 + RAD \rightarrow CO + O_2$	K78 = (2.5e-04 / 9.6e-03 / 2.2e-04 / 1.2e-08) s^{-1}	56.50	G12 (k20 > k78 > k87)	[5] gas-phase Employing $\Delta_r H$ from https://cccbdb.nist.gov/
$CO + O_3 \rightarrow CO_3 + O$	K79 = (2.1e-28 / 8.7e-26 / 2.0e-25 / 4.4e-26) cm^3 $molecule^{-1}$ s^{-1}	51.04	G10 (k22 > k79)	Employing $\Delta_r H$ from https://cccbdb.nist.gov/
$CO_3 + O \rightarrow CO + O_3$	K80 = (1.3e-26 / 1.5e-24 / 4.3e-26 / 2.8e-25) cm^3 $molecule^{-1}$ s^{-1}	− 51.04	G28 (k26 > k80)	Employing $\Delta_r H$ from https://cccbdb.nist.gov/
$O_2 + RAD \rightarrow O + O$	K81 = (4.1e-05 / 4.8e-03 / 8.0e-03 / <1.0e-08) s^{-1}	493.68	Single reaction pathway	[3, 4] gas-phase
$O + O \rightarrow O_2$	K82 = (8.4e-31 / 1.4e-27 / 7.9e-26 / 1.3e-25) cm^3 $molecule^{-1}$ s^{-1}	−493.68	Single reaction pathway	[3] surface [4] gas-phase; [11] ice and desorption
$O_3 + RAD \rightarrow O_2 + O$	K83 = (3.7e-05 / 1.7e-03 / 1.1e-04 / 1.2e-04) s^{-1}	102.44	G13 (k83 > k85)	[3,5] gas-phase [10] ice
$O_2 + O \rightarrow O_3$	k84 = (9.4e-28 / 8.3e-27 / 1.3e-26 / 6.6e-27) cm^3 $molecule^{-1}$ s^{-1}	−102.44	Single reaction pathway	[3] surface [11] ice and desorption
$O_3 + RAD \rightarrow O + O + O$	k85 = (3.7e-05 / 1.6e-03 / 7.6e-05 / 2.1e-05) s^{-1}	596.13	G13 (k83 > k85)	
$O + O + O \rightarrow O_3$	k86 = (8.5e-51 / 1.9e-49 / 2.1e-48 / 3.2e-49) cm^6 $molecule^{-2}$ s^{-1}	−596.13	Single reaction pathway	
$CO_3 + RAD \rightarrow CO + O + O$	k87 = (1.5e-05 / 4.0e-03 / 1.7e-04 / <1.0e-08) s^{-1}	573.17	G12 (k20 > k78 > k87)	Employing $\Delta_r H$ from https://cccbdb.nist.gov/
$CO + O + O \rightarrow CO_3$	k88 = (7.0e-53 / 2.7e-49 / 8.9e-50 / 6.1e-50) cm^6 $molecule^{-2}$ s^{-1}	−573.17	Single reaction pathway	Employing $\Delta_r H$ from https://cccbdb.nist.gov/
$C_2 + RAD \rightarrow C + C$	k89 = (3.4e-05 / 2.0e-03 / 1.5e-03 / 3.2e-04) s^{-1}	602.5	Single reaction pathway	[3, 5] gas-phase
$C + C \rightarrow C_2$	k90 = (7.6e-28 / 5.5e-26 / 1.9e-26 / 7.8e-26) cm^3 $molecule^{-1}$ s^{-1}	−602.5	Single reaction pathway	[3] surface [11] ice and desorption
$C_2O + RAD \rightarrow C + C + O$	k91 = (1.8e-04 / 1.7e-03 / 1.5e-04 / 9.3e-04) s^{-1}	1292.52	G14 (k66 > k91)	
$C + C + O \rightarrow C_2O$	k92 = (1.3e-48 / 3.1e-48 / 2.4e-49 / 3.9e-49) cm^6 $molecule^{-2}$ s^{-1}	−1292.52	Single reaction pathway	

Table 1 (*continued*)

Modelled reactions[a]	Effective rate constant (CR1 / CR2 / EL / UV)	Reaction enthalpy at 0 K[b] [kJ/mol]	Reaction groups (k values ordered based on reaction exothermicity) [c]	References or comments
$C_2O_2 + RAD \rightarrow C + CO + O$	k93 = (9.0e-06 / 1.0e-03 / 4.6e-04 / 2.5e-03) s^{-1}	830.4	G15 (k60 > k32 > k93)	
$C + CO + O \rightarrow C_2O_2$	k94 = (1.4e-48 / 4.5e-48 / 7.2e-50 / 2.3e-50) cm^6 $molecule^{-2}$ s^{-1}	−830.4	Single reaction pathway	
$C_2O_3 + RAD \rightarrow CO + CO + O$	k95 = (4.4e-05 / 2.3e-02 / 8.9e-04 / 2.2e-03) s^{-1}	301.4	G16 (k34 > k95 > k97 > k99)	Employing $\Delta_fH(C_2O_3)$ = -282.2 kJ mol-1 from Gambi et al. 2001
$CO + CO + O \rightarrow C_2O_3$	k96 = (2.1e-49 / 2.0e-48 / 1.6e-52 / 5.2e-49) cm^6 $molecule^{-2}$ s^{-1}	−301.4	single reaction pathway	Employing $\Delta_fH(C_2O_3)$ = -282.2 kJ mol-1 from Gambi et al. 2001
$C_2O_3 + RAD \rightarrow C_2O_2 + O$	k97 = (4.4e-05 / 1.7e-02 / 1.1e-04 / 2.2e-03) s^{-1}	543.0	G16 (k34 > k95 > k97 > k99)	Employing $\Delta_fH(C_2O_3)$ = -282.2 kJ mol-1 from Gambi et al. 2001
$C_2O_2 + O \rightarrow C_2O_3$	k98 = (1.7e-26 / 1.3e-25 / 1.6e-27 / 1.7e-25) cm^3 $molecule^{-1}$ s^{-1}	− 543.0	G17 (k36 > k98)	Employing $\Delta_fH(C_2O_3)$ = -282.2 kJ mol-1 from Gambi et al. 2001
$C_2O_3 + RAD \rightarrow C_2O + O_2$	k99 = (<1.0e-08 / 1.0e-03 / 1.1e-04 / 8.9e-04) s^{-1}	619.3	G16 (k34 > k95 > k97 > k99)	Employing $\Delta_fH(C_2O_3)$ = -282.2 kJ mol-1 from Gambi et al. 2001
$C_2O + O_2 \rightarrow C_2O_3$	k100=(5.0e-27 / 1.6e-25 / 4.3e-27 / 3.4e-25) cm^3 $molecule^{-1}$ s^{-1}	−619.3	G20 (k38 > k100)	Employing $\Delta_fH(C_2O_3)$ = -282.2 kJ mol-1 from Gambi et al. 2001
CO_2 (ice) + RAD → CO_2 (gas-phase)	$k_{des,CO2}$ = (2.2e-06 / 8.1e-05 / 9.3e-08 / 5.2e-05) s^{-1}	–	–	Intrinsic desorption rate
CO (ice) + RAD → CO (gas-phase)	$k_{des,CO}$ = (8.5e-07 / 7.7e-03 / 2.7e-07 / 1.6e-04) s^{-1}	–	–	Intrinsic desorption rate
CO_3 (ice) + RAD → CO_3 (gas-phase)	$k_{des,CO3}$ = (2.1e-06 / 1.2e-03 / 2.0e-07 / 5.8e-04) s^{-1}	–	–	Intrinsic desorption rate
O (ice) + RAD → O (gas-phase)	$k_{des,O}$ = (2.4e-05 / 1.7e-03 / 1.6e-07 / 2.7e-04) s^{-1}	–	–	Intrinsic desorption rate
O_2 (ice) + RAD → O_2 (gas-phase)	$k_{des,O2}$ = (2.4e-05 / 8.8e-04 / 2.9e-08 / 4.3e-04) s^{-1}	–	–	Intrinsic desorption rate
O_3 (ice) + RAD → O_3 (gas-phase)	$k_{des,O3}$ = (4.6e-06 / 2.2e-03 / 1.7e-07 / 2.8e-04) s^{-1}	–	–	Intrinsic desorption rate
C (ice) + RAD → C (gas-phase)	$k_{des,C}$ = (9.8e-06 / 3.5e-03 / 9.2e-08 / 8.7e-05) s^{-1}	–	–	Intrinsic desorption rate
C_2 (ice) + RAD → C_2 (gas-phase)	$k_{des,C2}$ =(1.4e-05 / 6.9e-03 / 6.1e-08 / 2.5e-04) s^{-1}	–	–	Intrinsic desorption rate
C_2O (ice) + RAD → C_2O (gas-phase)	$k_{des,C2O}$ = (1.7e-06 / 1.6e-03 / 5.2e-08 / 5.8e-04) s^{-1}	–	–	Intrinsic desorption rate
C_2O_2 (ice) + RAD → C_2O_2 (gas-phase)	$k_{des,C2O2}$ =(5.2e-07 / 4.6e-03 / 3.6e-08 / 2.5e-05) s^{-1}	–	–	Intrinsic desorption rate
C_2O_3 (ice) + RAD → C_2O_3 (gas-phase)	$k_{des,C2O3}$ = (9.0e-06 / 2.0e-03 / 2.2e-07 / 3.7e-04) s^{-1}	–	–	Intrinsic desorption rate
Molecular desorption[d] M (ice) + RAD → M (gas-phase)	Summed desorption rate = (4.1e + 11/ 1.3e + 14/ 1.7e + 11 /4.8e + 12) molecules s^{-1}Summed desorption yield = (4.9e + 03/ 8.0e-04/ 4.0e-01 /3.0e-02) molecules $projectile^{-1}$	–	–	[1,2] Summed desorption yield

[a]Calculated considering the total incoming projectiles and total desorbed species (employing the following experimental radiation flux:ϕ_{CR1} = 2x10^8 Ti ions cm^{-2} s^{-1}, ϕ_{CR2} = 2x10^9 Ni ions cm^{-2} s^{-1}, ϕ_{EL} = 16x10^{11} electrons cm^{-2} s^{-1} and ϕ_{UV} = 2x10^{14} photons cm^{-2} s^{-1}).

[b] For reactions enthalpy calculations it was considered only gas phase species and its lowest state energies in the calculation of the reaction enthalpy at 0 K; For the reactions involving CO_2, CO, O, O_2, O_3, C, C_2, C_2O, C_2O_2 it was employed the values $\Delta_fH(CO_2)$ = -393.1 kJ mol^{-1}; $\Delta_fH(CO)$ = -113.8 kJ mol^{-1}; $\Delta_fH(O_3)$ = 144.3 kJ mol^{-1}; $\Delta_fH(O)$ = 246.8 kJ mol^{-1}; $\Delta_fH(O_2)$ = 0 kJ mol^{-1}; $\Delta_fH(C)$ = 711.4 kJ mol^{-1}; $\Delta_fH(C_2)$ = 820.2 kJ mol^{-1}; $\Delta_fH(C_2O)$ = 337.1 kJ mol^{-1}; $\Delta_fH(C_2O_2)$ = 14 kJ mol^{-1}, obtained from the Active Thermochemical Tables version 1.122p https://atct.anl.gov/ (Ruscic et al. 2004; 2005; Ruscic and Bross 2020; Active Thermochemical Tables (ATcT) values based on ver. 1.122p of the Thermochemical Network (2020)); For the reactions involving CO_3 it was assumed the gas-phase formation enthalpies at 0 K of ΔfH = 52.5 kJ mol-1, and the reactions enthalpies ΔrH were obtained from the NIST website (https://cccbdb.nist.gov/); For the reactions involving C_2O_3 it was considered the $\Delta_fH(C_2O_3)$ = -282.2 kJ mol-1 (from Gambi et al. 2001) together with the other formations enthalpies from https://atct.anl.gov/);[c] As an hypothesis, we adopt a ranking of ERC based on the thermochemical data. The lowest value of reaction enthalpy (most exothermic reaction) should have the higher ERC (faster reaction) of the reaction group considered. The assignment "single reaction pathway" in this column indicates reactions which the reactants set appeared only once in this table.[d]The reaction order of each equation is assumed to be equal to the number of reactants molecules (for k1 to k100). For the desorption rates, it was considered first order reaction.

[1] Pilling et al. 2010a; [2] Martín-Doménech et al. 2015); [3] KIDA database (http://kida.astrophy.u-bordeaux.fr); [4] UMIST database (http://udfa.ajmarkwick.net); [5] NIST database (https://kinetics.nist.gov/kinetics/); [6] Bittner et al. 2020; [7] Cottin et al. 2003; [8] Gerakines et al. 1996.; [9] Okabe 1978; [10] Moll et al. 1966; [11] Hasegawa & Herbst 1993; [12] Raut & Baragiola 2011; [13] Goumans et al. 2008; In this manuscript it was only considered non-ionic reactions.

Table 2
Comparison between selected effective rate constants (ERCs) with rate constants at solid-phase from literature.

Selected reactions[a]	Solid-phase effective rate constants (ERCs) in pure CO_2 ice (CR1 / CR2 / EL / UV) (this work)	Solid phase rate constant (literature)	Notes and references (literature)
$CO_2 + RAD \rightarrow CO + O$	k1 = (3.1e-06 / 9.4e-07 / 1.6e-06 / 1.3e-08) s^{-1}	–	–
$CO_2 + EL \rightarrow CO + O$	–	~ 1.7e-5 s^{-1}[b]	[1]; from the irradiation of CO_2: $C^{18}O_2$ (1:2) at 10 K by 5 keV electrons.
$CO_2 + EL \rightarrow X$	–	~ 4e-5 s^{-1}[b]	[1]; from the irradiation of CO_2: $C^{18}O_2$ (1:2) at 10 K by 5 keV electrons.
$CO_2 + CR \rightarrow X$	–	3.6e-4 s^{-1}[c]	[3]; from the irradiation of CO_2 at 13 K by 52 MeV ions.
$CO_2 + CR \rightarrow X$	–	3.4e-4 s^{-1}[c]	[4]; from the irradiation of CO_2 at 13 K by 46 MeV Ni ions.
$CO + RAD \rightarrow C + O$	k57 = (3.5e-06 / <1.0e-08 / 7.5e-08 / <1.0e-08) s^{-1}	–	–
$CO + EL \rightarrow X$	–	2.9e-4 s^{-1} [d]	[2]; from the irradiation of CO ice at 15 by keV electrons;
$CO + EL \rightarrow X$		~4.2e-5 s^{-1} [e]	[6] [1] from the irradiation of ^{13}CO: $C^{18}O$ (1:1) at 10 K by 5 keV electrons.
$CO + CR \rightarrow X$	–	1e-4 s^{-1}[c]	[5] from the irradiation of CO ice 13 K 50 MeV Ni ions.
$CO + CR \rightarrow X$	–	3e-5 s^{-1}[c]	[5] from the irradiation of CO ice at 13 K 537 MeV Ni ions.

[a] X indicates a unspecified product.
[b] Rates from the average destruction of CO_2 and $C^{18}O_2$. In this model all reactions were considered of first order (distributed in one, two and three steps mechanisms).
[c] k calculated from the multiplication of ion flux and dissociation cross section (determined from associative exponential function to the experimental data).[d] Occurs in the presence of additional CO (excited) species yielding typically CO_2 and C. It was considered pseudo-first-order reaction for the produced CO_2. The CO_2 is not destroyed or does not react once produced. Other reactions in the model are all of first order.[e] Obtained from the average values of destruction of ^{13}CO and $C^{18}O$. It was considered only first order and pseudo-first-order reactions in the chemical network.
[1] Bennett et al (2010); [2] Jamieson et al. (2006); [3] Pilling et al. (2010a). [4] Seperuelo-Duarte et al. (2009); [5] Seperuelo-Duarte et al. (2010); [6] Bennett et al (2009).

Additionally, in our methodology, we do not consider individual activation energies once such quantities in solid-phase are highly dependent on the chemical environment, local temperature, and density (see also Alves et al. 2021; Pilling and Bonfim, 2020). Since the studied CO_2 ices (and the astrophysical ices in general) are continuously exposed to radiation, the incoming energy (and also the distributed energy within the ice by the fast secondary electrons) would allow exceeding most of the reactions´ activation barriers.

In spite of the remaining limitations of the code (e.g. limited number of species and chemical reactions), we expect the current results to be more realistic than the previous version, even understanding that solid-phase thermochemistry data (usually difficult to be determined experimentally and to be calculated) should be different from gas-phase and that some reaction might have an activation barrier. However, the issue about the presence of activation barrier can be exceeded in these irradiated ices if we consider that there is enough energy in the sample due to the incoming ionizing radiation (cosmic rays, fast electrons or UV). A comparison with previous model without the ordering of rate constants (Pilling et al. 2022a), focused on the CR2 and UV models, is also provided and similarities and differences are discussed.

3. Results and discussion

The PROCODA code employed in this work is a powerful tool for the characterization of laboratory studies that perform monitoring of irradiated ices by infrared spectroscopy (e.g. Grim & d'Hendecourt 1986; Ioppolo et al. 2011; Garrod & Pauly 2011; d'Hendecourt et al. 1985; Gerakines et al. 1996; Jimenez-Escobar et al. 2016; Pilling et al. 2009; Pilling et al. 2010a,b, Öberg et al. 2009; Kaiser & Roessler 1998; Moore & Hudson 1998; Hudson & Moore 2001; Baratta et al. 2002; Gerakines et al. 2004; Bennett et al. 2006; Pilling et al. 2010a, 2010b; Ioppolo et al. 2011; Andrade et al. 2013; Almeida et al. 2014; de Barros et al. 2014; Portugal et al. 2014; Boduch et al. 2015; Martín-Doménech et al. 2015; Pilling et al. 2013; Pilling & Bergantini 2015; Suhasaria et al. 2017; Linnartz & Salama 2020; Sie et al. 2019; Tsuge et al. 2020; Mifsud et al. 2022a; Mifsud et al. 2022b; Palumbo 1997; Fillion et al. 2014).

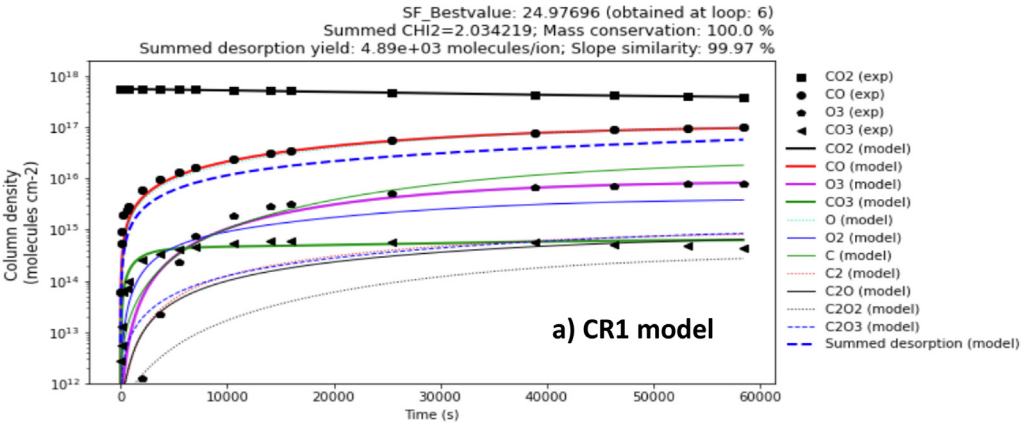
SF_Bestvalue: 24.97696 (obtained at loop: 6)
Summed CHI2=2.034219; Mass conservation: 100.0 %
Summed desorption yield: 4.89e+03 molecules/ion; Slope similarity: 99.97 %
Column density (molecules cm-2)
Time (s)
a) CR1 model
CO2 (exp)
CO (exp)
O3 (exp)
CO3 (exp)
CO2 (model)
CO (model)
O3 (model)
CO3 (model)
O (model)
O2 (model)
C (model)
C2 (model)
C2O (model)
C2O2 (model)
C2O3 (model)
Summed desorption (model)

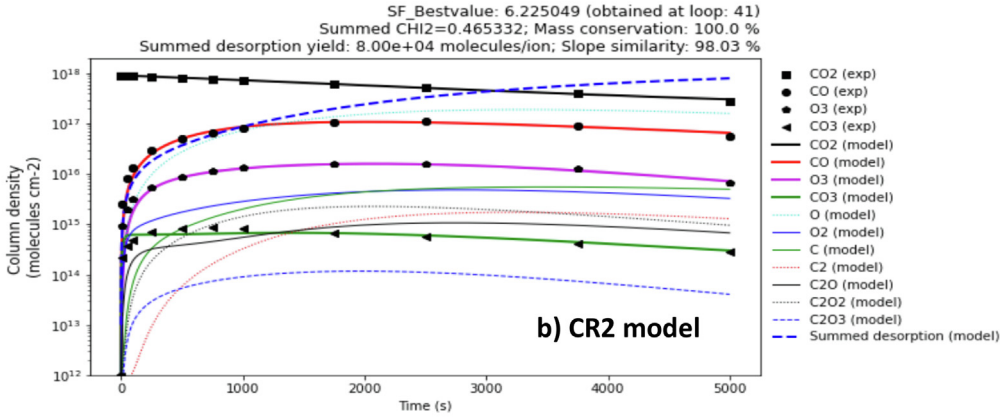
SF_Bestvalue: 6.225049 (obtained at loop: 41)
Summed CHI2=0.465332; Mass conservation: 100.0 %
Summed desorption yield: 8.00e+04 molecules/ion; Slope similarity: 98.03 %
Column density (molecules cm-2)
Time (s)
b) CR2 model
CO2 (exp)
CO (exp)
O3 (exp)
CO3 (exp)
CO2 (model)
CO (model)
O3 (model)
CO3 (model)
O (model)
O2 (model)
C (model)
C2 (model)
C2O (model)
C2O2 (model)
C2O3 (model)
Summed desorption (model)

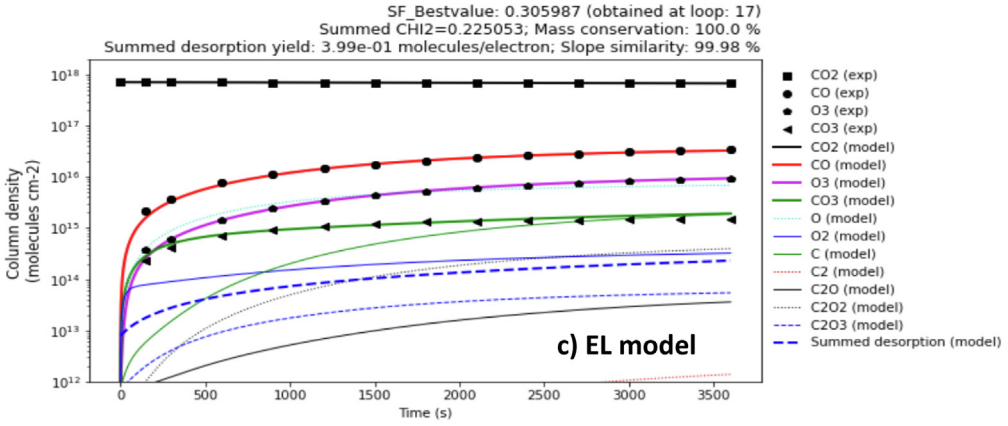
SF_Bestvalue: 0.305987 (obtained at loop: 17)
Summed CHI2=0.225053; Mass conservation: 100.0 %
Summed desorption yield: 3.99e-01 molecules/electron; Slope similarity: 99.98 %
Column density (molecules cm-2)
Time (s)
c) EL model
CO2 (exp)
CO (exp)
O3 (exp)
CO3 (exp)
CO2 (model)
CO (model)
O3 (model)
CO3 (model)
O (model)
O2 (model)
C (model)
C2 (model)
C2O (model)
C2O2 (model)
C2O3 (model)
Summed desorption (model)

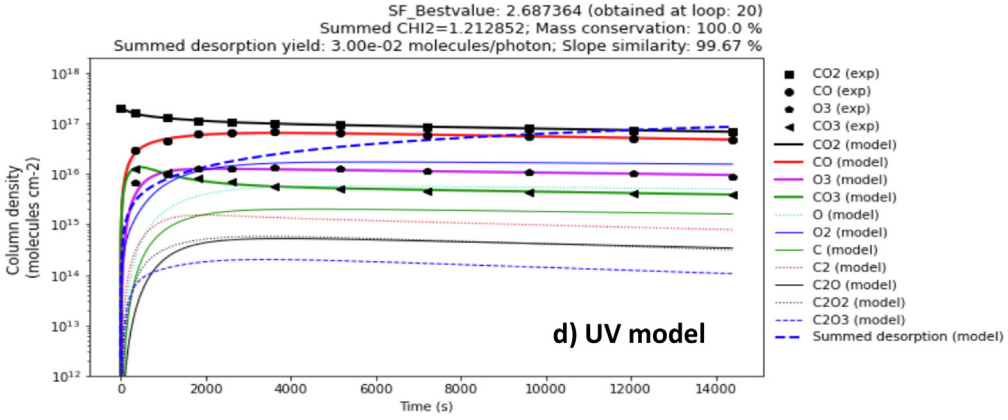
SF_Bestvalue: 2.687364 (obtained at loop: 20)
Summed CHI2=1.212852; Mass conservation: 100.0 %
Summed desorption yield: 3.00e-02 molecules/photon; Slope similarity: 99.67 %
Column density (molecules cm-2)
Time (s)
d) UV model
CO2 (exp)
CO (exp)
O3 (exp)
CO3 (exp)
CO2 (model)
CO (model)
O3 (model)
CO3 (model)
O (model)
O2 (model)
C (model)
C2 (model)
C2O (model)
C2O2 (model)
C2O3 (model)
Summed desorption (model)

Additionally, the code also can be very useful to help the prediction and the identification of molecules in astronomical observations (e.g. Gerakines et al. 1999; Pontoppidan et al. 2008; Evans et al. 2009, Ehrenfreund & Charnley 2000; Fraser et al. 2002; van Dishoeck 2014; Boogert et al. 2015; Tielens 2013; Kwok 2016). In addition, the ERCs calculated by the code can also be used in astrochemical models to help to understand the chemical evolution of cold space environments (e.g. Wakelam et al. 2010; Holdship et al. 2018; Shingledecker et al. 2019; Heyl et al. 2020; Rocha et al. 2022).

In this section, we will present the main results of the employ of the upgraded PROCODA code to map the chemical evolution of CO_2 ices exposed to ionizing radiation.

3.1. Evolution of molecular abundances and effective rate constants (ERCs)

Fig. 2 shows the evolution of column density, obtained for the best-fit models employing the upgraded PROCODA code in the irradiated pure CO_2 ices by different ionizing agents at low temperature. Panels a, b, c and d presents the different models: CR1 model (employing 550 MeV Ti ions), CR2 model (52 MeV Ni ions), EL model (5 keV electrons), and UV model (10 eV photons), respectively. In this figure the experimental data are given by black symbols, the calculated model are given by lines (with the thick lines being the model for the observed species), and the dashed thick blue line is modeled summed desorption. In all panels, important output parameters for the best-fit models are displayed in the header, including the values of chi-squared function χ^2 (sometimes also named here as summed CHI2).

The models are in a very good match with the experimental data and also reproduce the CE behavior (a slighted sloped plateau observed at large fluences). As discussed by Pilling et al. (2022a), with this methodology, we are able to quantify both the abundances of observable and non-observed species in the IR spectra irradiated ices. Such characterization helps us to better understand the underlying chemistry within the ice during the laboratory experiments and also helps to put constrain in astrochemical observations.

It is worth noting that even though each of these reactions may occur within different chemical environments (surrounded by different molecular arrangements), which also change over time, only a single reaction rate constant is given per reaction, which does not change over time, and therefore the values in this table are actually the effective rate constants (ERCs) for the entire irradiation process. The term "effective" employed in the ERCs is also employed to take into account ices inhomogeneities in chemistry which locally affect the chemical environment and ice properties, in another word, to account in some way for an average value within the ice (see also Alves et al. 2021; Pilling and Bonfim 2020). Additional details about the model parameters can be obtained at Pilling et al. (2022a) and Carvalho et al. (2022).

Comparing the current CR2 and UV models with the its previous versions, which do not employ any thermochemistry data (Pilling et al. 2022a), showed that current models have better accuracy. This was observed in the value of chi-squared function (χ^2) which decreased by 22 % (from $\chi^2 = 0.59$ to 0.46) and 36 % (from $\chi^2 = 1.95$ to 1.25) in the current CR2 and UV model, respectively, compared with previous version. Additionally, the parameter *SSC,* employed to guarantee the CE condition at larger fluences, was closer to 100 % in the current version, which also indicates an improvement in the solution of coupled chemical system.

Table 1 lists the considered chemical reaction routes in this work and the calculated ERC obtained by employing the upgraded PROCODA code taking into account the ERC ordering hypothesis based on thermochemistry data (where reactions with smaller ΔH (more exothermic) are expected to have larger ERCs (or k), being faster). The thermochemistry data employ literature 0 K gas-phase data for the considered reaction network. The employed reactions set include 11 direct reactions, 69 bimolecular reactions, 11 termolecular reactions, and 11 desorption reactions. The reaction enthalpy and the numbering of the considered reaction groups (with the ERCs ordering based on the reaction exothermicity) are also listed. The intrinsic values for molecular desorption are listed at the bottom of the table. The estimated errors for these rates are below 20 % as discussed by Pilling et al. (2022a).

From Table 1 we notice that some individual reactions are highly endothermic (at gas-phase), which would be also very difficult to occur at low temperature when considered isolated in the ice. However, due to the constant input energy in the ices (which also increase local temperature at the collision point), such endothermic reaction might have a chance to occur overpassing this endothermic

Fig. 2. The evolution of column density obtained for the best-fit models employing the upgraded PROCODA code on pure CO_2 ices irradiated by different ionizing agents at low temperature. Panel a, b, c and d presents the CR1 model (550 MeV Ti ions; Mejía et al. 2015), CR2 model (52 MeV Ni ions; Pilling et al. 2010a), EL model (5 keV electrons; Bennett et al. 2004), and UV (10 eV photons; Martín-Doménech et al. 2015), respectively. The black symbols represent the experimental data (observed molecular abundances for CO_2, CO, O_3 and CO_3). The bold-dashed blue line represents the summed desorption column density calculated in each model. In all panels, important output parameters for the best-fit models are displayed in the header.

threshold. Additionally, readers should have in mind that in this work, we describe a set of coupled reactions that occur simultaneously in the ice bulk under bombardment, and reactions in the solid phase behave differently than in the gas phase (they are dependent on neighborhood properties as well as the configuration of neighbor molecules (see also Alves et al. 2021; Pilling and Bonfim 2020)). This also strengthens the employ of the term ERC in this study instead of only rate constant.

Fig. 3 presents, for comparison purposes, the values of the calculated ERC obtained by the best-fit models employing the current PROCODA code (with the ordering hypothesis for ERCs based on thermochemistry data) in the pure CO_2 ices irradiated by different ionizing agents (CR1 model: 550 MeV Ti ions, CR2 model: 52 MeV Ni ions, EL model: 5 keV electrons; UV model: 10 eV photons). Panel a, b, c and d presents the ERC for the direct, the bimolecular, the termolecular and the intrinsic desorption reactions induced by radiation, respectively. The estimated errors for these rates are below 20 % as discussed by Pilling et al. (2022a). The numerical values of this figure are listed in Table 1.

The average values for the ERCs (with the standard deviation error) obtained with the current methodology on pure CO_2 ices under the presence of different ionizing agents is shown in Fig. 4. The panels a, b, c, and d present the average ERCs for the direct, the bimolecular, the termolecular and the radiation-induced intrinsic desorption reactions, respectively. The CR2 model presents the higher value for the average direct, bimolecular and termolecular ERCs and the UV model presents the lowest average values. The calculated average ERCs for the direct dissociation reaction were 6.4e-4, 7.5e-3, 2.1e-3 and 1.6e-3 s^{-1} for the CR1, CR2, EL and UV models, respectively. For the bimolecular reactions, the calculated average ERCs were 1.0e-26, 2.4e-25, 1.3e-25 and 1.0e-25 cm^3 $molecule^{-1}$ s^{-1}, for the CR1, CR2, EL and UV models, respectively. For the termolecular reactions, the calculated average ERCs were 6.7e-49, 8.6e-48, 2.3e-48 and 4.8e-49 cm^6 $molecule^{-2}$ s^{-1}, for the CR1, CR2, EL and UV models, respectively. A comparison, between the ERC obtained in the current model with the previous one (Pilling et al. 2022a) showed that the average values (only for CR2 and UV) for the direct and bimolecular reactions presented roughly double the previous calculated value. Curiously, for the termolecular rates the comparison with previous calculation shows that the current CR2 model average value is roughly 8 times higher and the UV model average value is double.

The PROCODA code recently was also applied to describe the molecular evolution on pure acetonitrile (CH_3-CN) ice irradiated by X-rays (Carvalho et al. 2022). In this research, the authors employ 273 reaction rates involving 33 molecular species (5 species observed in the experiment and 28 non-observed or unknown) and they determined the average values for dissociation, bimolecular, and termolecular ERCs of 2.3e − 3 s^{-1}, 9.7e − 26 cm^3 $molecules^{-1}$ s^{-1} and 3.2e − 47 cm^6 $molecules^{-2}$ s^{-1}, respectively.

In general, the average ERCs (with exception for the intrinsic desorption rate) for the EL model lay between the values obtained in the CR2 and UV model indicating that for these three ionizing agents the higher projectile energy the higher is the molecular ERC. Additionally, the average intrinsic desorption rate constant for the electrons was the higher among the studied ionized agents which might be a consequence of the employed experiment technique that is different from the other data (infrared data obtained in the reflection mode and not by transmission mode). A comparison between the two models employing cosmic rays shows that the CR1 model presents the lower average values for the ERC than the values found for the CR2 model, which might be attributed to the different interaction cross sections of the penetration length of projectiles (also associated with different values of stopping power; see details at Pilling et al. 2010b).

It is worth noting that the destruction cross-section for CO_2 obtained from the experiments employing 550 MeV Ti ions (Mejía et al. 2015) is lower than the value obtained employing 52 MeV Ni ions (Pilling et al. 2010a), 7e-14 cm^{-2} and 1.8e-13 cm^{-2}, respectively. This rule was true for the summed desorption yield determined experimentally in these works, which indicates that the value was lower for 550 MeV Ti ions than for 52 MeV Ni ions (around 1.3e4 and 2.2e4 molecules ion^{-1}, respectively).

The current average ERC values for the intrinsic desorption were 8.4e-6 s^{-1}, 2.9e-3 s^{-1}, 1.2e-7 s^{-1} and 2.8e-4 s^{-1}, for the CR1, CR2, EL and UV models, respectively. Such values (in the case of Ni ions and UV photons) were around 80 % higher than the obtained by previous calculations (see Pilling et al. 2022a). This indicates that the employ of ERCs ordering hypothesis by thermochemical data induced changes also in the way intrinsic desorption was quantified since some reaction have preferences than another. Moreover, since the current model has a better chi-squared function (χ^2) than the previous model, we argue that current intrinsic desorption values are also more accurate.

Comparisons between selected ERCs obtained with the current methodology with some rate constants taken from literature, in both solid and gas phases, are provided in Tables 2 and 3, respectively. Table 2 compares selected ERCs (mainly CO_2 and CO direct reactions) with some rate constants at solid-phase taken from literature which describes a simple kinetic model to map chemical evolution of CO_2 (Bennett et al. 2010) and CO ices (Bennett et al. 2009; Jamieson et al. 2006), both irradiated by keV electrons. Differently to the current work, which considers, direct, bimolecular, termolecular and radiation-induced desorption reactions, the described literature models employ a number of reactions and chemical species smaller than in the current work, and additionally, all reactions were considered to be of the first order (distributed in one, two and three steps mechanisms). The ERC for the direct dissociation reaction of CO_2 to CO + O, obtained in the current methodology for the EL model was only

one order of magnitude lower than calculated by Bennett et al. (2010). This table also presents some rate constants determined directly from the experimental papers employing cosmic ray analogs (calculated from the experimental "effective" destruction cross-section) taken from Pilling et al. (2010) and Seperuelo-Duarte et al. (2009).

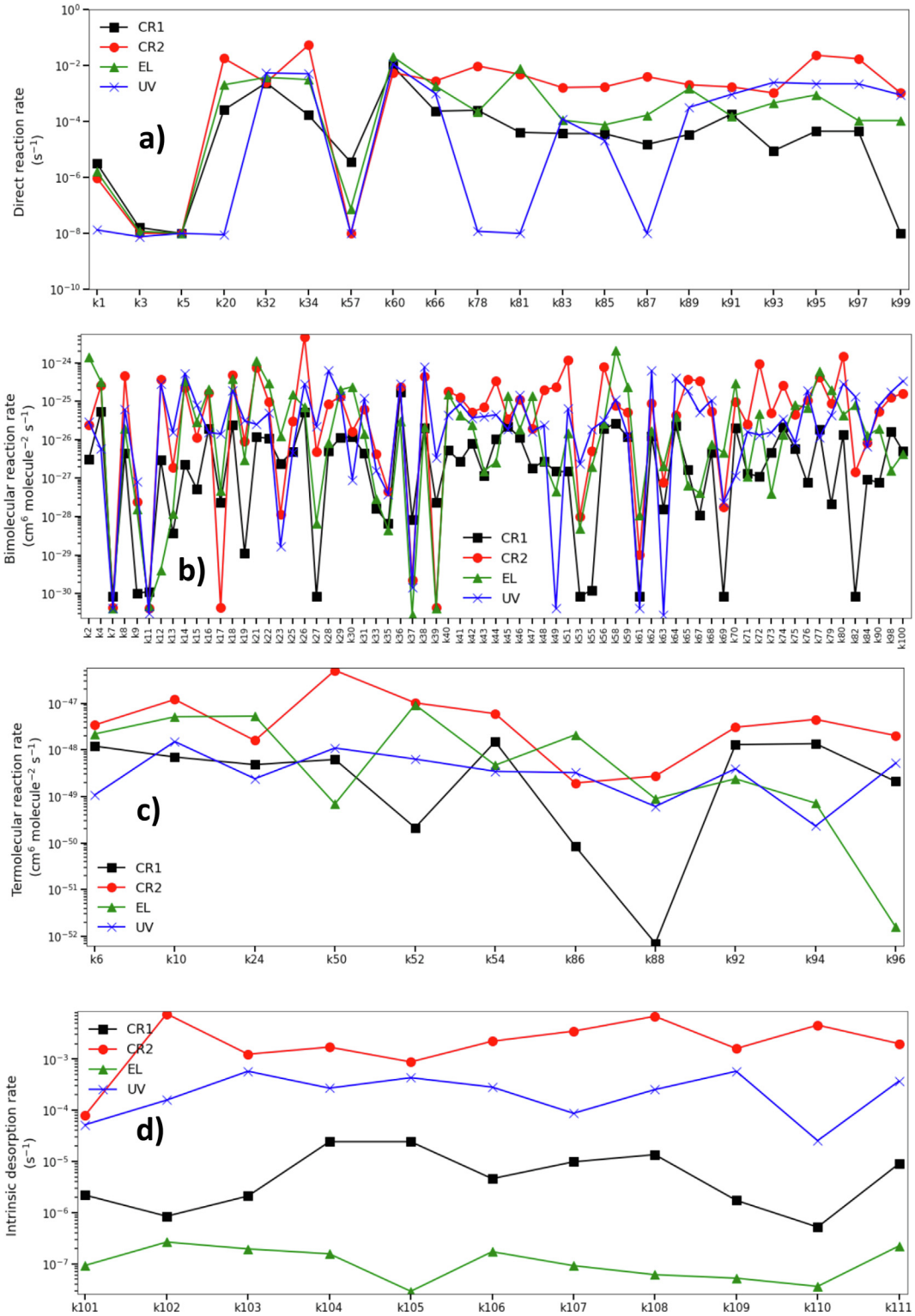

Fig. 3. Values for the effective rate constants (ERCs) obtained by the best-fit models employing current version of the PROCODA code in the irradiated pure CO_2 ices by different ionizing agents (CR1: 550 MeV Ti^{+21}, CR2: 52 MeV Ni^{+13} EL: 5 keV electrons; UV: 10 eV photons). Panel a, b, c and d presents the ERCs values for the direct, the bimolecular, the termolecular and the radiation-induced intrinsic desorption reactions, respectively. The numerical values of this figure are listed in Table 1.

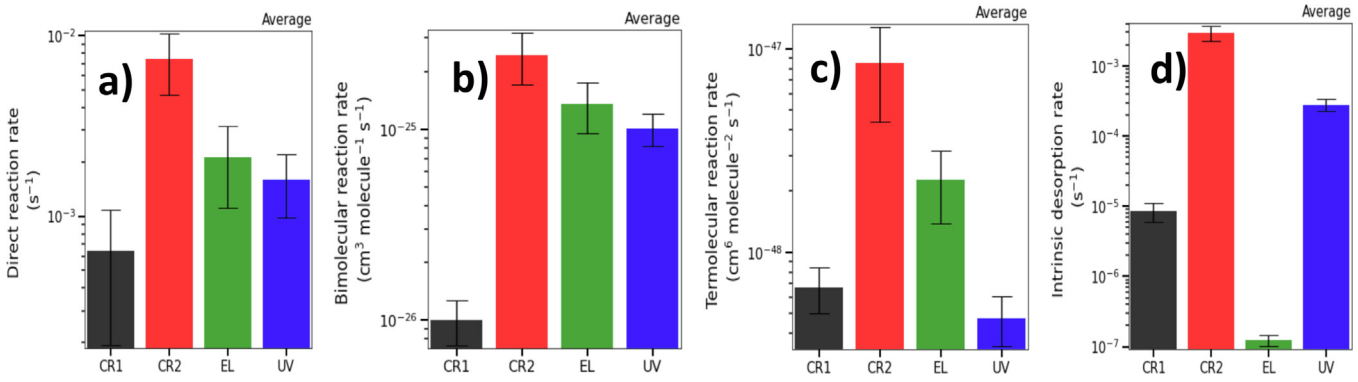

Fig. 4. Comparison between the average values of the effective rate constants (ERCs) employing the upgraded PROCODA code (with the ordering hypothesis for ERCs based on thermochemistry data) in the irradiated pure CO_2 ices. Panel a, b, c and d present the average values (with the standard deviation error) of the ERCs in the direct dissociation reactions, bimolecular reactions, thermolecular reactions and intrinsic radiation-induced desorption reactions, respectively. (CR1 model: 550 MeV Ti ions, CR2 model: 52 MeV Ni ions, EL model: 5 keV electrons; UV model: 10 eV photons).

It is worth noting that the current ERC for direct radiation-induced reactions of a given species A (e.g. *A + RAD → products*) takes into account also excitation processes triggered by the incoming radiation itself also from the collision with secondary electrons within the ice, leading to the given product (e.g. *A + RAD → A* → products*). Such considerations for the excited species are also employed in the calculations of bimolecular and termolecular reactions. Details of such excitation process are described, for example, by Jamieson et al. (2006) and Bennett et al (2010).

Table 3 presents, for a comparison purpose, the ERCs for selected reactions obtained with current methodology with some rate constants at gas-phase taken from different works in the literature (e.g. Mallard et al. 1994; Gredel et al. 1989, van Dishoeck, 1988; van Dishoeck et al. 2006; Husain & Young 1975). For direct reactions, the values determined here (independently of the ionizing radiation employed) are much higher than the gas-phase values. Probably, this issue is due to the fact that ERC handle several processes at the same time, also involving ionic and excited states and also involving the collision with secondary electrons within the ice bulk, making the reaction faster than gas phase. Such phenomenon was previously discussed by Pilling et al. (2011) during a comparison of dissociation cross sections of organic species during bombardments of ices and gases by X-rays.

For bimolecular reactions, the calculated values for the ERC presented here are several orders of magnitude smaller than in the values at gas-phase, and this is probably related with the difficulty in the mobility and the diffusion of reactants within the ice bulk. The small values found, in comparison with the gas-phase, may also indicate that such collision processes should play a smaller role in ice chemistry; however it is worth noting that some new produced molecular species (e.g. C_2O_2) only can be explained by invoking such collision reactions within the ices.

3.2. Branching ratio within the considered reaction groups

As discussed in the methodology in the current manuscript we considered a rate constant ordering hypothesis based on gas-phase thermochemistry at 0 K (most exothermic reactions should be faster). In this section, we present

Table 3
Comparisons between selected effective rate constants (ERCs) in ices with rate constants at gas-phase.

Selected reactions	Solid-phase effective rate constants (ERCs) in pure CO_2 ice (CR1 / CR2 / EL / UV) (this work)	Gas-phase rate constant[a] (literature)	Notes and references (literature)
$CO + RAD \rightarrow C + O$	k57 = (3.5e-06 / 1.0e-08 / 7.5e-08 / <1.0e-08) s^{-1}	1.30e-17 s^{-1}	[2] Cosmic ray
		2.00e-10 s^{-1}	[3] UV photons
$CO_2 + RAD \rightarrow CO + O$	k1 = (3.1e-06 / 9.4e-07 / 1.6e-06 / 1.3e-08) s^{-1}	1.30e-17 s^{-1}	[2] Cosmic ray
		8.90e-10 s^{-1}	[4] UV photons
$O_2 + RAD \rightarrow O + O$	K81 = (4.1e-05 / 4.8e-03 / 8.0e-03 / <1.0e-08) s^{-1}	1.30e-17 s^{-1}	[2] Cosmic ray
$CO + O_2 \rightarrow CO_2 + O$	k16 = (1.9e-26 / 1.7e-25 / 2.0e-25 / 1.5e-26) cm^3 molecule^{-1} s^{-1}	5.99E-12 cm^3 molecule^{-1} s^{-1}	[1] Theoretical
$CO_2 + O \rightarrow O_2 + CO$	k15 = (5.3e-28 / 1.1e-26 / 3.0e-26 / 8.0e-26) cm^3 molecule^{-1} s^{-1}	2.46E-11 cm^3 molecule^{-1} s^{-1}	[1] Theoretical
$CO_2 + C \rightarrow C_2O_2$	k31 = (4.4e-27 / 6.3e-26 / 1.4e-26 / 1.2e-25) cm^3 molecule^{-1} s^{-1}	< 1E-14 cm^3 molecule^{-1} s^{-1}	[5] Under UVC photolysis
$C_2O + O \rightarrow CO + CO$	k64 = (2.3e-26 / 4.3e-26 / 4.0e-26 / 4.0e-25) cm^3 molecule^{-1} s^{-1}	8.59E-11 cm^3 molecule^{-1} s^{-1}	[1] Theoretical

[a] Employing only the α term only in the Arrhenius-type formulae (see McElroy et al. 2013).[1] UMIST databse; Mallard et al. 1994; [2] UMIST database, Gredel et al. 1989; [3] UMIST database; van Dishoeck, 1988;
[4] UMIST database; van Dishoeck et al. 2006; [5] Husain & Young 1975.

the branching ratio within the considered reaction groups (named from G1 to G28). For comparison purposes, we present in the values between brackets, the branching ratio obtained in the previous PROCODA code version without rate constant ordering hypothesis (Pilling et al. 2022a) for the CR2 and UV. It is worth noting that for some reaction groups (<2% of the calculations) the ERCs ordering hypothesis was not strictly respected during the algorithm minimization to obtain the best-fit solutions (values marked with asterisks in this section). This issue could be due to a minimization algorithm rounding procedure or a small dependence of such reactions in the entire reactions set.

3.2.1. Groups of reaction pathways containing CO_2 as one of reactants

Reaction group G1 (with rate constant ordering hypothesis: k1 > k3 > k5)

$$CO_2 + RAD \xrightarrow{k_1(CR1=99.1\%/CR2=98\%[89.7\%]/EL=98.6\%/UV=42.5\%[33.3\%])} CO + O$$

$$\xrightarrow{k_3(0.5\%/1.1\%[5.8\%]/0.8\%/24.8\%[33.3\%])} C + O_2$$

$$\xrightarrow{k_5(0.4\%/0.9\%[4.5\%]/0.6\%/32.7\%[33.3\%])} C + O + O$$

Reaction group G2 (k13>k9>k11>k7)

$$CO_2 + CO_2 \xrightarrow{k_7(2.1\%/\ 0\%[0.2\%]/0.1\%/\ 0\%[\ 0\%])} C_2O_2 + O_2$$

$$\xrightarrow{k_9(2.5\%/11.2\%[94.3\%]/55.4\%*/5.1\%[\ 0\%])} CO + CO + O_2$$

$$\xrightarrow{k_{11}(2.8\%/\ 0\%[\ 0\%]/0.2\%/\ 0\%[\ 0\%])} C_2O_3 + O$$

$$\xrightarrow{k_{13}(92.6\%/88.8\%[5.5\%]/44.3\%/94.9\%[100\%])} CO_3 + CO$$

Reaction group G3 (k15>k19>k17)

$$CO_2 + O \xrightarrow{k_{15}(67.9\%/55.0\%[41.9\%]/89.6\%/64.0\%[48.5\%])} CO + O_2$$

$$\xrightarrow{k_{17}(30.7\%*/\ 0\%[30.7\%]/1.5\%/11.2\%[\ 0\%])} C + O_3$$

$$\xrightarrow{k_{19}(1.4\%/45.0\%[27.4\%]/8.9\%/24.8\%[51.5\%])} CO_3$$

Reaction group G4 (k21>k25>k23)

$$CO_2 + O_2 \xrightarrow{k_{21}(62.5\%/96.1\%[89.7\%]/87.1\%/84.1\%[61.9\%])} CO + O_3$$

$$\xrightarrow{k_{23}(12.5\%/\ 0\%[7.1\%]/1.0\%/0.1\%[\ 0\%])} C + O + O_3$$

$$\xrightarrow{k_{25}(25.0\%/3.9\%[3.1\%]/11.9\%/15.8\%[38.1\%])} CO_3 + O$$

Reaction group G5 (k29>k31>k27)

$$CO_2 + C \xrightarrow{k_{27}(\ 0\%/2.4\%[98.0\%]/\ 0\%/7.8\%[62.9\%])} C_2 + O_2$$

$$\xrightarrow{k_{29}(71.4\%/65.7\%[2.0\%]/93.4\%/49.7\%[28.6\%])} CO + COCO + CO$$

$$\xrightarrow{k_{31}(28.6\%/31.8\%[\ 0\%]/6.5\%/42.5\%[8.5\%])} C_2O_2$$

Reaction group G6 (k33>k35>k37>k39)

$$CO_2 + CO \xrightarrow{k_{33}(29.8\%/90.5\%[5.2\%]/86.4\%/29.7\%[25\%])} C_2O_3$$

$$\xrightarrow{k_{35}(12.2\%/9.5\%[\ 0\%]/13.4\%/7.2\%[25\%])} C_2O_2 + O$$

$$\xrightarrow{k_{37}(15.2\%/0.1\%[\ 0\%]/0.1\%/\ 0\%[25\%])} C_2O + O_2$$

$$\xrightarrow{k_{39}(42.8\%*/\ 0\%[94.8\%]/0.1\%/63.1\%*[25\%])} C_2 + O_3$$

Reaction group G7 (k51>k49)

$$CO_2 + CO_3 \xrightarrow{k_{49}(49.9\%/16.1\%[30.9\%]/3.0\%/\ 0\%[\ 0\%])} C_2O + 2\,O_2$$

$$\xrightarrow{k_{51}(50.1\%/83.9\%[69.1\%]/97.0\%/100\%[100\%])} 2\,CO + O_3$$

Reaction group G21 (k41>k43)

$$CO_2 + C_2O \xrightarrow{k_{41}(71.1\%/65.3\%[15.0\%]/96.5\%/68.3\%[38.3\%])} C_2O_2 + CO$$

$$\xrightarrow{k_{43}(28.9\%/34.7\%[85.0\%]/3.5\%/31.7\%[61.7\%])} C_2O_3 + C$$

Reaction group G23 (k55>k53)

$$CO_2 + O_3 \xrightarrow{k_{53}(41.2\%/1.9\%[95.1\%]/2.4\%/11.8\%[6.2\%])} CO + O_2 + O_2$$

$$\xrightarrow{k_{55}(58.8\%/98.1\%[4.9\%]/97.6\%/88.2\%[93.8\%])} CO_3 + O_2$$

Reaction group G25 (k45>k47)

$$CO_2 + C_2 \xrightarrow{k_{45}(92.4\%/63.0\%[99.2\%]/50.1\%/52.9\%[95.2\%])} CO + C_2O$$

$$\xrightarrow{k_{47}(7.6\%/37.0\%[0.8\%]/49.9\%/47.1\%[4.8\%])} C_2O_2 + C$$

3.2.2. Groups of reaction pathways containing CO as one of reactants

Reaction group G6 (see reactions with CO_2)

Reaction group G8 (k2 > k69)

$$CO + O \xrightarrow{k_2(100\%/99.3\%[11.6\%]/99.7\%/99.2\%[100\%])} CO_2$$

$$\xrightarrow{k_{69}(\ 0\%/0.7\%[88.4\%]/0.3\%/0.8\%[\ 0\%])} C + O_2$$

Reaction group G10 (k22 > k79)

$$CO + O_3 \xrightarrow{k_{22}(98.1\%/53.2\%[25.6\%]/59.2\%/52.2\%[55.3\%])} CO_2 + O_2$$

$$\xrightarrow{k_{79}(1.9\%/46.8\%[74.4\%]/40.8\%/47.8\%[44.7\%])} CO_3 + O$$

Reaction group G11 (k59 > k30 > k63 > k61)

$$CO + CO \xrightarrow{k_{30}(49,7\%/24.4\%[43.5\%]/49.7\%/6.5\%[25\%])} CO_2 + C$$

$$\xrightarrow{k_{59}(49,8\%/74.5\%[\ 0\%]/49.8\%/93.5\%[25\%])} C_2O_2$$

$$\xrightarrow{k_{61}(\ 0\%/\ 0\%[35.2\%]/\ 0\%/\ 0\%[25\%])} C_2 + O_2$$

$$\xrightarrow{k_{63}(0.5\%/1.1\%[21.3\%]/0.5\%/\ 0\%[25\%])} C_2O + O$$

Reaction group G18 (k46 > k73)

$$CO + C_2O \xrightarrow{k_{46}(70.1\%/69.6\%[92.3\%]/97.9\%/89.7\%[30.0\%])} CO_2 + C_2$$

$$\xrightarrow{k_{73}(29.9\%/30.4\%[7.7\%]/2.1\%/10.3\%[70.0\%])} C_2O_2 + C$$

Reaction group G19 (k77 > k16 > k75)

$$CO + O_2 \xrightarrow{k_{16}(43.2\%/26.3\%[56.0\%]/23.0\%/43.6\%*[\ 0\%])} CO_2 + O$$

$$\xrightarrow{k_{75}(13.5\%/7.1\%[1.9\%]/9.1\%/24.4\%[\ 0\%])} C + O_3$$

$$\xrightarrow{k_{77}(43.3\%/66.6\%[42.1\%]/67.9\%/32.0\%[100\%])} CO_3$$

Reaction group G26 (k65 > k67)

$$CO + C \xrightarrow{k_{65}(93.9\%/52.1\%[\ 0\%]/61.7\%/78.5\%[74.1\%])} C_2O$$

$$\xrightarrow{k_{67}(6.1\%/47.9\%[100\%]/38.3\%/21.5\%[25.9\%])} C_2 + O$$

3.2.3. Other reaction groups

Reaction group G13 (k83 > k85)

$$O_3 + RAD \xrightarrow{k_{83}(50.1\%/51.5\%[54.9\%]/59.1\%/85.1\%[97.9\%])} O_2 + O$$

$$\xrightarrow{k_{85}(49.9\%/48.5\%[45.1x\%]/40.9\%/14.9\%[2.1\%])} O + O + O$$

Reaction group G22 (k18 > k76)

$$C + O_3 \xrightarrow{k_{18}(96.9\%/81.35\%[97.7\%]/85.0\%/50.1\%[55.1\%])} CO_2 + O$$

$$\xrightarrow{k_{76}(3.1\%/19.0\%[2.3\%]/15.0\%/49.9\%[44.9\%])} CO + O_2$$

Reaction group G12 (k20>k78>k87)

$$CO_3 + RAD \xrightarrow{k_{20}(49.5\%/56.9\%[0.2\%]/83.7\%/29.0\%[0.3\%])} CO_2 + O$$

$$\xrightarrow{k_{78}(47.6\%/30.4\%[46.1\%]/9.2\%/38.7\%*[2.1\%])} CO + O_2$$

$$\xrightarrow{k_{87}(2.9\%/12.7\%[53.7\%]/7.1\%/32.3\%[97.6\%])} CO + 2O$$

Reaction group G27 (k74>k48)

$$C_2O_2 + C \xrightarrow{k_{48}(11.4\%/42.2\%[52.9\%]/16.7\%/40.7\%[50\%])} CO_2 + C_2$$

$$\xrightarrow{k_{74}(88.6\%/57.8\%[47.1\%]/83.3\%/59.3\%[50\%])} CO + C_2O$$

Reaction group G28 (k26>k80)

$$CO_3 + O \xrightarrow{k_{26}\ (80.3\%/75.8\%\ [45.8\%]\ /62.3\%\ /50.1\%[71.6\%])} CO_2 + O_2$$

$$\xrightarrow{k_{80}(19.7\%/24.2\%[54.2\%]/37.7\%/49.9\%[28.4\%])} CO + O_3$$

A comparison between current CR2 and UV models with the previous models which do not have the hypothesis for ERCs ordering (Pilling et al. 2022a), in which the values are indicated by the values between brackets, suggests that changes in the ordering for ERC is more recurrent in case of CR2 model (observed in 46 % of the reaction groups in comparison with previous model: G2, G5, G6, G8, G10, G11, G12, G19, G21, G23, G26, G27 and G28). For the current UV model it was observed that 32 % of the reaction groups (G1, G3, G6, G11, G12, G18, G19, G21 and G27) presented changes in the ERC´s ordering in comparison with the previous model. At 18 % of the reaction groups (G4, G7, G13, G22, and G25) the ordering of reactions was unaltered within the reaction groups, by comparing current and previous code version. However, it is worth noting that even in these groups, the individual values of each ERC has changed.

A detailed physicochemical discussion about the dominant reactions in each case and why the branching ratio of specific reactions changes with the incoming radiation is out of the scope of this manuscript and should be done in future publications.

3.3. Radiation-induced molecular desorption

Fig. 5 presents the radiation-induced desorption column density and the intrinsic molecular desorption for the best-fit models obtained in this work. The CR2 and UV models have presented similar behavior for the desorption column density with a rapid enhancement of CO desorption after the beginning of irradiation becoming the dominant desorption species at the CE. For the CR2 model the four most largely desorbed species at the CE were CO, O, CO_2 and O_3 (in this order). For the UV model the four most important desorbed species at the CE were CO, CO_2, O_2 and O_3 (in this order). For the CR1 model the four most important desorbed species at the CE were CO_2, O, CO and CO_3 (in this order). Curiously, this indicated that depending on the type/energy of incident cosmic ray on given astrophysical ice this could yield a different molecular desorption scheme. The EL model present a desorption profile quite different than the other models being the CO_2 species dominant one during the entire irradiation, as well as, at the CE phase.

As observed also by Pilling et al (2022a), the ordering of the desorption column density for the considered species in the irradiated CO_2 ices changed as function of time during the irradiation, in which some species playing an important role in specific moments (e.g. O and CO in the CR2 model; O_2, O_3 and CO_3 in the UV model). Curiously, this behavior was not seen in the EL model which might be related with low penetration of incoming electrons in the ice. The changing in the desorption column density ordering with time also indicates that gaseous atmosphere in the vicinity of icy grains in space evolved, as function of time, until the CE phase is reached. This will be investigated with details in future investigation.

A comparison with previous models without the ordering hypothesis for ERCs (Pilling et al. 2022a) shows similar behavior in the desorption column density with some punctual differences in the molecular desorption ordering at the CE phase. Changes were also observed in the intrinsic molecular desorption between these two approaches (in the UV model mainly for CO, O, C_2O_2 and C_2O_3, and in the CR2 model mainly for the species CO_3, O, O_2, C_2 and C_2O). The current UV model have presented the same summed desorption yield (3e-2 molecules/photons) than previous UV model. For the CR2 model we observed a small decrease (<10 %) by comparing the summed desorption yield in the current code version (8e+4 molecules/ion) with the previous version.

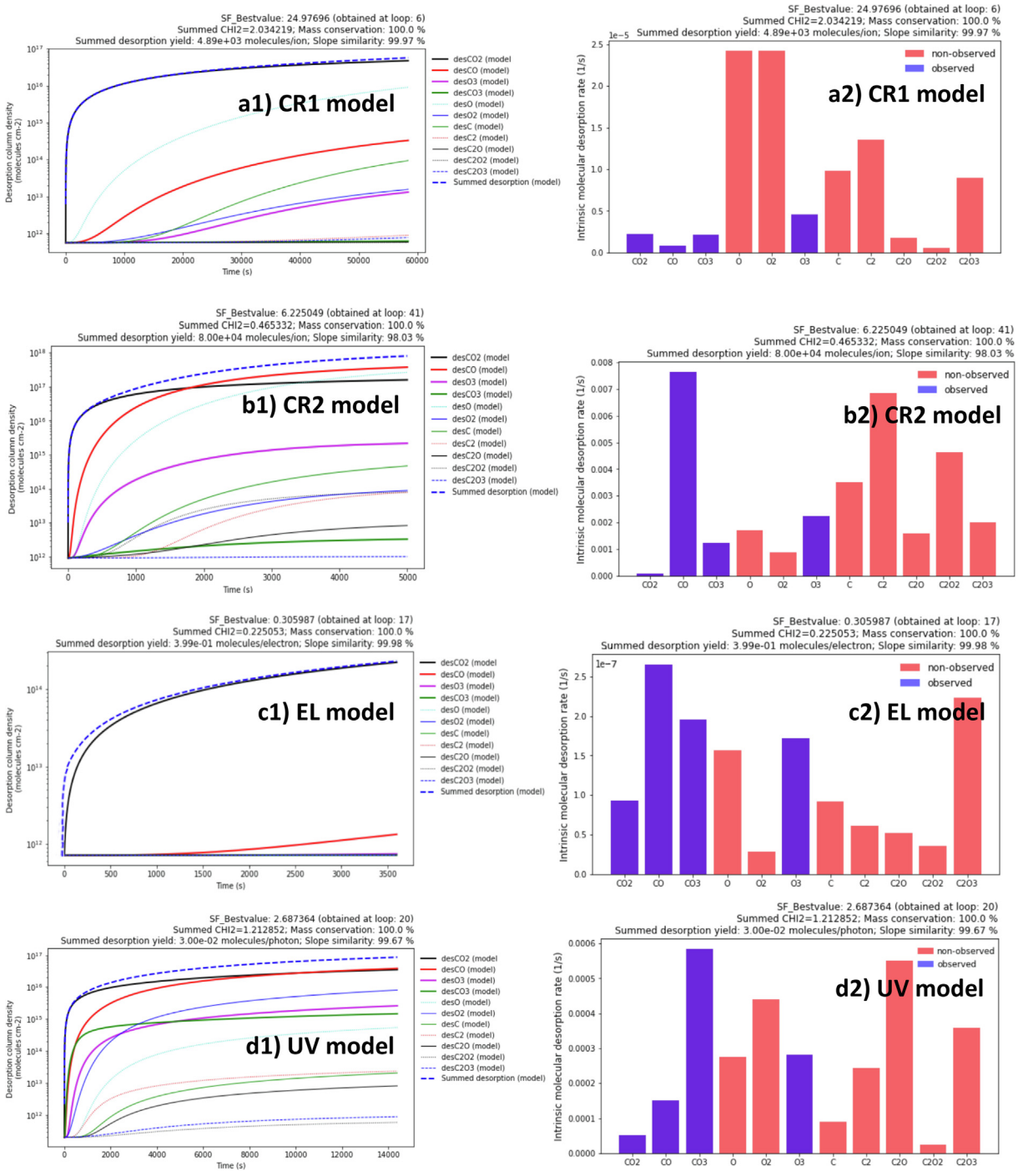

Fig. 5. Molecular desorption plots of best-fit models employing the upgraded PROCODA code. Left panels present the desorption column density for the modeled species with the summed value given by bold-dashed blue lines. Right panels present the intrinsic molecular desorption effective rate constant (DERC) for each modeled chemical species. Panels a, b, c and d presents the different models (CR1 model: 550 MeV Ti ions, CR2 model: 52 MeV Ni ions, EL model: 5 keV electrons; UV model: 10 eV photons), respectively.

Finally, it worth noting that in the current calculations we do not differentiate the desorbed species from the sputtered species (important in the case of cosmic rays). Moreover, the calculations not take into account specific desorption mechanisms, or reactive desorption species or excited states. Here, we considered only that all species that go to the gas phase (removed from the ice) are desorbed species.

3.4. The chemical equilibrium (CE) phase

The CE phase (or stage) of irradiated astrophysical ices occurs when the variation of summed chemical abundances is negligible, which happens at larger radiation fluences. In this situation, which requires an ice at constant temperature, the production and consumption of a given species are virtually equal, which keep chemical abundances nearly

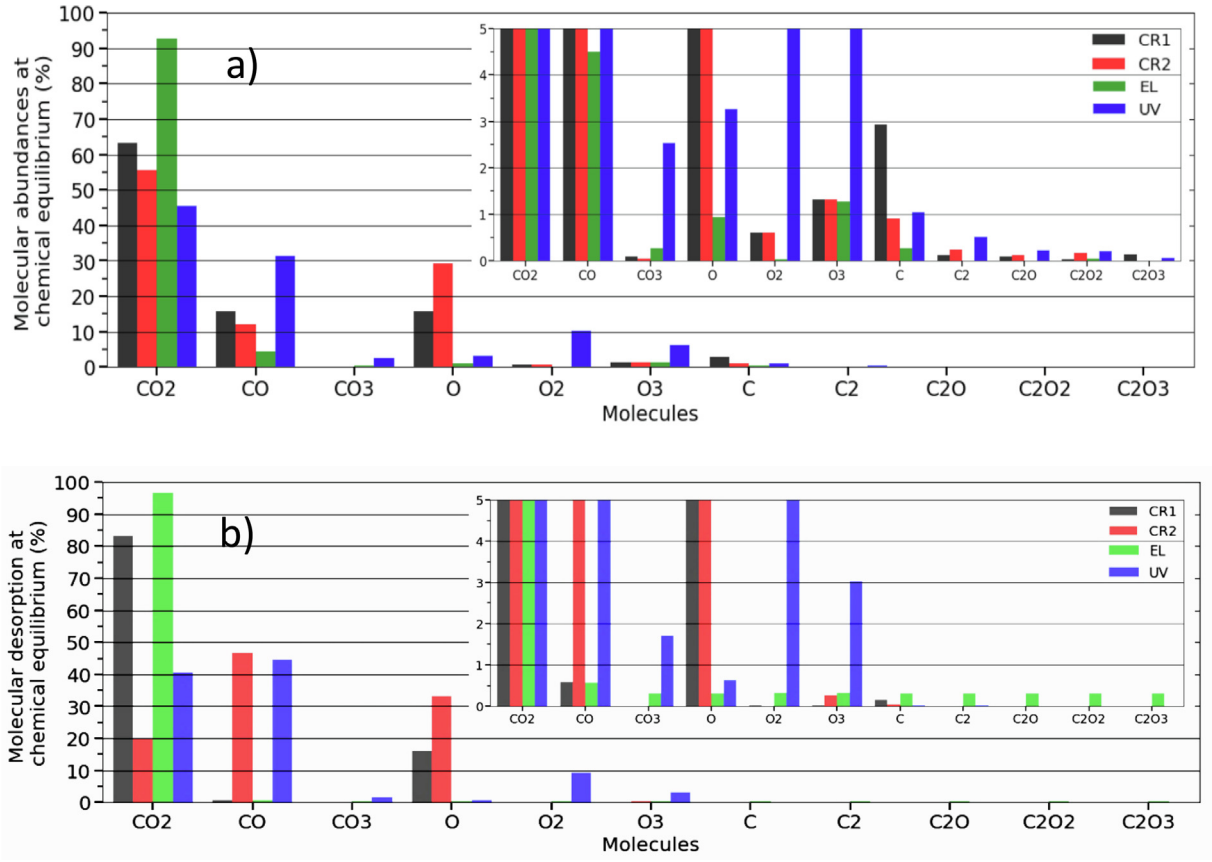

Fig. 6. Percentage values for the molecular abundances (panel a) and molecular desorption (panel b) at chemical equilibrium for the studied pure CO_2 ices irradiated by different ionizing radiation, obtained the upgraded PROCODA code (with the ordering of ERC for selected reactions based on thermochemistry data). The inset panel in each figure is a zoom of the main figure for percentages below 5%. (CR1 model: black color, CR2 model: red color, EL model: green color, UV model: blue color).

constant (e.g. Almeida et al. 2017; de Souza Bonfim et al. 2017; Rachid et al. 2017; Vasconcelos et al. 2017a, 2017b, 2017c) It is worth noting that the CE phase depends on the initial molecular abundances, the ice temperature and type of incoming ionizing radiation (as is observed in this manuscript). This phase also characterizes a certain timescale in the ice's life (named timescale to reach the CE phase) where the changes in chemical abundances in an astrophysical ice remains nearly unaltered even after extended irradiation (see also Carvalho & Pilling 2020a, 2020b; Freitas & Pilling 2020, Pilling et al. 2022a).

Fig. 6 shows, in percentage, the molecular abundances (panel a) and molecular desorption (panel b) at CE phase, obtained with the upgraded version of PROCODA code. Each color indicates a specific model studied in this manuscript (CR1 model: black color, CR2 model: red color, EL model: green color, UV model: blue color). It is worth noting that the presented percentages were calculated directly from the values of molecular column densities at the CE phase. From Fig. 6a, we observe that in all models the CO_2 species is the most abundant one in the CE phase, being considerably more abundant in the case of experiments employing electrons (92.6 %). The second most abundant species was the CO in most experiments, excepting in the case of CR2 model which was the oxygen atoms (29.1 %) a non-observed species in the ice. It is worth noting that the abundances at the CE phase for the species CO, O, C_2 and O_3, are considerably larger in the UV model than in the other models, which can help to constrain the main radiation field in the processing of ices within different astrophysical regions. Fig. 6a also highlights an enhanced production of O atoms (and also C atoms) in the ices irradiated by CRs, which might be related with the larger destruction of eventual new-produced species such as CO (the dominant product when UV photon is applied), O_2, O_3 and C_2.

The desorption column density at the CE, in percentage, shown in Fig. 6b suggests that the experiments can be separated into two different groups: group A – large desorption of parental species (the case of CR1 and EL models) and group B – large desorption of the daughter species CO (for CR2 and UV models). Table 4 list the values of molecular abundances, in percentage, determined at the CE employing the upgraded PROCODA for the studied CO_2 ices. The values between brackets, presented for comparison purposes, result for the CR2 and UV models obtained in previous calculation without the ordering hypothesis for ERCs (Pilling et al. 2022a).

A comparison between current CR2 and UV models with respective models performed with the previous code version (Pilling et al. 2022a) shows good similarities in the case of UV model and some interesting differences in the case of CR2 model (the current model yields, at the CE phase, almost the double of CO_2 species and a very small content of O_2, C and C_2 with respect to the previous model). Important differences were also observed in the amount of summed observed and non-observed species in the ice in the current CR2 model with respect to the previous model. This comparison indicates, once more, that the ordering ERCs by thermochemistry data is more relevant when more energy is deposited in the sample. It is worth noting that the model that presents the largest and the lowest abundance of the parent species in the CE phase was the EL model and UV model, respectively. Both cosmic ray models presented the largest production of O atoms, being the lowest production observed in the EL model (the same behavior was also observed for C atoms). The largest production of O_3 was observed in the UV model, being the other models presenting curiously similar abundances in the CE phase (1.3 %). The formation of O_2 molecule seems to be much enhanced when UV photons is employed in respect with other ionization sources. Finally, we highlight that the differences in the abundances observed at CE phase might help to put constrain in astrophysical models depending on the dominant type of incoming radiation in a given astrophysical icy scenario.

Table 5 present the values of molecular desorption, in percentage, at the CE phase obtained in the best-fit models employing the upgraded PROCODA code at four irradiated pure CO_2 ices. The values between brackets, presented for comparison purposes, results for the CR2 and UV models obtained in the previous calculation without the ordering hypothesis for ERCs (Pilling et al. 2022a). A comparison between current CR2 and UV models with the previous models shows good similarities in the case of UV models and some interesting differences in the case of CR2 models (main differences occur for desorption of CO, O, and C). Important differences were also observed in the amount of summed observed and non-observed species in the ice in the current CR2 model with respect to the previous model, indicating that desorption in current model is much more ruled by observed species, an opposite behavior from previous model. This comparison indicates that the ordering of ERCs values by thermochemistry data is much more important for the ices that are exposed to higher energy delivered as the case of CR2 model in respect with the UV model.

3.5. Effective equilibrium constant for the irradiated ice

When a simple chemical system reaches the CE phase involving only one forward–backward reaction

$$\sum r_i R_i \underset{k_{bck}}{\overset{k_{for}}{\rightleftarrows}} \sum p_i P_i \tag{3}$$

where R_i and P_i indicate the different reactants and products species (with r_i and p_i its respective stoichiometric coefficient in the reaction) and k_{for} and k_{bck} being the rate constant for the forward and backward reactions, respectively, we can write a thermodynamic parameter called chemical equilibrium constant K following the equation

$$K = \frac{k_{for}}{k_{bck}} = \frac{\prod [P_i]^{p_i}}{\prod [R_i]^{r_i}} \tag{4}$$

where $[R]^{ri}$ and $[P]^{pi}$ indicate the concentration of a given reactant and product at equilibrium, in units of column density, with its respective stoichiometric coefficient in the reaction, respectively.

Depending on the value of K we can state that the CE phase is reactant-favored (for $K < 1$) or product-favored (for $K > 1$). The chemical equilibrium constant is related with other important thermodynamics parameters of the system such as the change in the Gibbs free energy ΔG ("the available energy") or the changes in the enthalpy ΔG and entropy ΔS by the equation

$$K = e^{\left(\frac{-\Delta G}{RT}\right)} = e^{\left(\frac{-\Delta H + T\Delta S}{RT}\right)} \tag{5}$$

where R is the perfect-gas constant (8.314 J K^{-1} mol^{-1}) and T is the temperature in kelvin. Additionally, since K is related with entropy changes it helps to understand also the evolution of the chemical complexity of the system (e.g. Atkins et al. 2014).

In the case of coupled and multiple equations the equilibrium constant of the ice system K_{ice} can be written as

$$K_{ice} = \prod_{i=1}^{n} K_i = \prod_{i=1}^{n} \frac{k_{i,for}}{k_{i,bck}} = \prod_{i=1}^{n} \left(\frac{\prod [P_i]^{p_i}}{\prod [R_i]^{r_i}} \right) \left[\text{molecules cm}^{-2}\right]^{\Delta n} \tag{6}$$

where $[R]^{ri}$ and $[P]^{pi}$ indicate the concentration of a given reactant and product at equilibrium, in units of column density, with its respective stoichiometric coefficient in the reaction, respectively (adapted from Flowers et al. 2015). In this equation K_i represents the equilibrium constant of each pair of forward-reverse reaction employing in the current model (excluding the desorption reactions). It is worth noting that the unit of the equilibrium constant is given by (molecules cm^{-2})$^{\triangle n}$, where $\Delta n = 1$ is obtained by the sum of stoichiometric coefficients of products minus the sum of stoichiometric coefficients of reactants.

Considering that in the current work we employ 50 pair of forward–backward reactions (described in the Table 1 from k1 to k100; were k2 is the reverse of k1, k4 is the reverse of k3 and so on) we can write the equilibrium constant of the ice system as multiplication of 50 quotients as is illustrated shortly by

Table 4
Value of molecular abundances (in number of molecules) of frozen species, in percentage, at the CE phase obtained in the best-fit models employing the upgraded PROCODA code in the four irradiated pure CO_2 ices.

Molecular species	CR1 Model	CR2 Model[b]	EL Model	UV Model[b]
CO_2[a] (parent)	63.2 %	55.6 % [33.8 %]	92.6 %	45.5 %[41.5 %]
CO[a]	15.6 %	11.9 % [7.9 %]	4.5 %	31.3 %[29.7 %]
CO_3[a]	0.1 %	<0.1 % [<0.1 %]	0.3 %	2.5 %[2.2 %]
O	15.9 %	29.1 % [30.4 %]	0.9 %	3.3 %[3.8 %]
O_2	0.6 %	0.6 % [3.1 %]	<0.1 %	10.2 %[14.9 %]
O_3[a]	1.3 %	1,3% [0.9 %]	1.3 %	6.2 %[5.8 %]
C	2.9 %	0.9 % [23.1 %]	0.3 %	1.1 %[0.8 %]
C_2	0.1 %	0.2 % [0.8 %]	~0%	0.5 %[0.3 %]
C_2O	0.1 %	0.1 % [0.1 %]	~0%	0.2 %[0.4 %]
C_2O_2	<0.1 %	0.2 % [~0%]	<0.1 %	0.2 %[0.1 %]
C_2O_3	0.1 %	~0% [~0%]	~0%	<0.1 % [0.5 %]
Summed observed species	**80.2 %**	**68.9 %[42.6 %]**	**98.7 %**	**85.5 %[79.2 %]**
Summed non-observed species	**19.8 %**	**31.1 %[57.4 %]**	**1.3 %**	**14.5 %[20.8 %]**

[a] Observed species by FTIR.
[b] The values between brackets, presented for comparison purpose, results for the CR2 and UV models obtained in previous calculation without the ordering hypothesis for ERCs (Pilling et al. 2022a).

Table 5
Values of molecular desorption, in percentage, at the CE phase obtained in the best-fit models employing the upgraded PROCODA code in the four irradiated pure CO_2 ices.

Molecular species	CR1 Model	CR2 Model[b]	EL Model	UV Model[b]
CO_2[a] (parent)	83.2 %	19.8 % [15.6 %]	96.6 %	40.6 % [25.5 %]
CO[a]	0.6 %	46.7 % [12.2 %]	0.6 %	44.6 % [61.1 %]
CO_3[a]	~0%	~0% [~0%]	0.3 %	1.7 % [0.9 %]
O	15.9 %	33.1 %[57.4 %]	0.3 %	0.6 % [0.7 %]
O_2	<0.1 %	~0% [0.3 %]	0.3 %	9.4 % [10.9 %]
O_3[a]	<0.1 %	0.3 % [0.1 %]	0.3 %	3.0 % [0.9 %]
C	0.2 %	<0.1 % [14.3 %]	0.3 %	<0.1 % [<0.1 %]
C_2	~0%	~0%[<0.1 %]	0.3 %	<0.1 % [~0%]
C_2O	~0%	~0%[~0%]	0.3 %	~0% [~0%]
C_2O_2	~0%	~0%[~0%]	0.3 %	~0% [~0%]
C_2O_3	~0%	~0%[~0%]	0.3 %	~0% [~0%]
Summed observed species	**83,9%**	**66.8 % [27,9%]**	**97.8 %**	**89.9 % [88.4 %]**
Summed non-observed species	**16.1 %**	**33.2 % [72.1 %]**	**2.2 %**	**10.1 % [11.6 %]**

[a] Observed species by FTIR.
[b] The values between brackets, presented for comparison purpose, results for the CR2 and UV models obtained in previous calculation without the ordering hypothesis for ERCs (Pilling et al. 2022a).

$$K_{ice} = K_1K_2K_3\cdots K_{50} = \left(\frac{[CO][O]}{[CO_2]}\right)\left(\frac{[C][O_2]}{[CO_2]}\right)\left(\frac{[C][O]^2}{[CO_2]}\right)\cdots\left(\frac{[C_2O][O_2]}{[C_2O_3]}\right) \quad (7)$$

However, since in the studied ices here the CO_2 species is the original parent species, we can write the forward–backward reaction to describe the CE phase considering the CO_2 the only reactant species being the other species named as the products. After making the stoichiometric balance of the combined forward–backward full reactions (employing the entire reaction set, excluding the desorption reactions) we can write an effective forward–backward reaction in the chemistry equilibrium as

$$[CO_2]^{11} \underset{k_{bck}}{\overset{k_{for}}{\rightleftarrows}} [CO][CO_3][O][O_2][O_3]^3[C][C_2][C_2O][C_2O_2] \times [C_2O_3] \quad (8)$$

In short, eq. (8) presents the simplest effective forward–backward reaction that describes the ice system under irradiation in the chemical equilibrium phase (consider all modelled species). This procedure not considers any desorption reactions from ice to gas-phase. It is worth noting that there were other possibilities to write the effective forward–backward reaction in the chemistry equilibrium (see eq. (8)) considering 11 CO_2 molecules as reactants, for example, the ones obtained by changing the term $[O][O_2][O_3]^3$, in the products, by $[O]^2[O_2]^2[O_3]^2$,

$[O][O_2]^4[O_3]$, $[O]^3[O_2]^3[O_3]$, $[O]^5[O_2]^2[O_3]$ or$[O]^7[O_2][O_3]$. However such alternative combinations suggest a strongly product-favored chemical network in the equilibrium which is not observed in the models as we detailed bellow.

Considering eq. (8), as the representative for effective forward–backward reaction that describes the ice system under irradiation in the chemical equilibrium phase we can obtain the effective equilibrium constant of the frozen system by

$$K_{ice} = \left(\frac{[CO][CO_3][O][O_2][O_3]^3[C][C_2][C_2O][C_2O_2][C_2O_3]}{[CO_2]^{11}}\right)[moleculescm^{-2}] \quad (9)$$

where the abundances for the considered species at the CE are in units of column density. Employing the values of column density at the CH phase obtained from the models in this equation, we calculate the effective equilibrium constant $K_{ice} = 1.7e\text{-}7$, 6.4e-8, 2.0e-20, 3.2e0 molecules cm^{-2}, for the CR1, CR2, EL, UV models, respectively. This indicates that the CE phase in the considered network is strongly reactant-favored for the CR1, CR2 and EL models (mainly this model), however it is virtually neutral (neither side favored) for the UV model (see also Silberberg, 2012).

In this work, we consider eq. (9) as the representative one for the effective forward–backward reaction in the chemistry equilibrium (the one with the lowest possible amount of products) because the effective equilibrium constant obtained employing the other discussed possibilities (different products combinations) suggest an strongly product-favored chemical network in the equilibrium which is not observed in the models (see Fig. 2).

4. Astrochemical implications

As discussed previously, carbon dioxide is one of the important species in space, widely observed in molecular clouds. The quantification of its chemical pathways in the solid phase under the presence of ionizing radiation such as UV photons, swift electrons or CRs is essential to better understand the redistribution of carbon in the ISM since CO_2 holds a large reservoir of depleted carbon in astrophysical ices. Additionally, the CO_2 bending mode is an important diagnostic tracer of the ice structure and temperature (e.g. Chiar et al. 1995, Ehrenfreund et al. 1997; Pontoppidan et al. 2003; Baratta & Palumbo 2017).

As reported by Öberg et al. (2011), CO_2 is the second most abundant frozen molecule with respect to H_2O ice as observed toward low-mass protostars (29 %), and quiescent molecular clouds (38 %), and it has abundance similar to CO ice toward high-mass protostars (13 %). However, depending on the object, the carbon monoxide abundances may overpass the CO_2 abundant in gas-phase space (see also Huang et al. 2020). The employ of PROCODA to map the chemical evolution of CO ice exposed to ionizing radiation in the laboratory (pure CO ice at 13 K irradiated by 50 MeV Ni ions) was recently submitted for publication (Pilling et al. 2022b). This work found that the most abundant species, at the CE phase, for such experimental data were atomic oxygen (68.2 %) and atomic carbon (18.2 %), followed by CO (11.8 %) and CO_2 (1.6 %).

While some computational codes simulating surface chemical reactions have been made available (e.g., Ruaud et al. 2016, Holdship et al. 2017), they mostly rely on reaction rates of gas-phase molecules, which may lead to inaccurate results. In this paper, we present new reaction rates (presented in terms of effective rate constants, ERCs) focusing on the CO_2 ice chemistry triggered by ionizing radiation at different energy levels (2 different types of cosmic rays, UV and 5 keV electrons). The upgrade in the PROCODA code allows to ordering the chemical reactions using thermochemistry data, and consequently, accurate physicochemical parameters can be calculated. Additionally, the current improvements added in the code contributes to decrease the inaccuracies of chemical reactions triggered by photons, electrons or ions in frozen CO_2, as well its daughters species, in the astrochemical models. Therefore, the main astrochemical implication of current work is the claim for the employ of these calculated values of ERC in an astrochemical models. This will better describe astrochemical ices under processing by radiation and also better describe desorption of specific compounds to gas-phase induced by the incoming radiation in the ices.

Additionally, the characterization of the CE phase for the CO_2 ices under the presence of different ionizing fields provide by this work show interesting aspects. For example, this species is much more consumed in the ices when 52 MeV Ni ions impinge the ices in comparison with the 550 MeV Ti ions. At this phase the production of CO is almost the same under the presence of both UV and 52 MeV Ni ions. The production of O_2 and O_3 is enhanced in the presence of UV photons but the production of O is enhanced in the presence of CRs. Additionally from the analysis of branching ratio of reactions within the studied reaction groups we outline that some reactions are much more important depending on the incoming radiation (See details in section 3.1). It is worth noting that combining the quantification of chemical abundances of ices taken from space observations (such the ones performed by the JWST) with the molecular abundances quantified for the CE phase (perfumed in the current work) may also help to constrain the type and the role of the incoming ionizing radiation field in a given observed astrophysical ice/region.

Among the species studied in this work, there are three of them that we would like to highlight their astrochemical relevance: C_2O, C_2O_2, and C_2O_3 (see structures at Fig. 1). The species C_2O is a linear molecule that is of interest in many areas. However, despite its simplicity, it is a very reactive species that is not encountered commonly, being detected for the first time in space environments at the cold dark molecular cloud TMC-1 (e.g. Ohishi et al. 1991). It is called an oxocarbon and can be used as a building block to synthesize oxocarbon anions (Seitz and Imming, 1992).

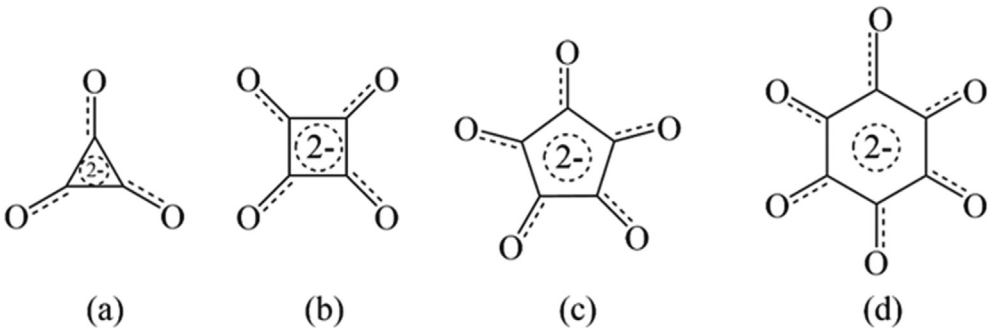

Fig. 7. Structures of oxocarbon anions. (a) deltate, (b) squarate, (c) croconate and (d) rhodizonate.

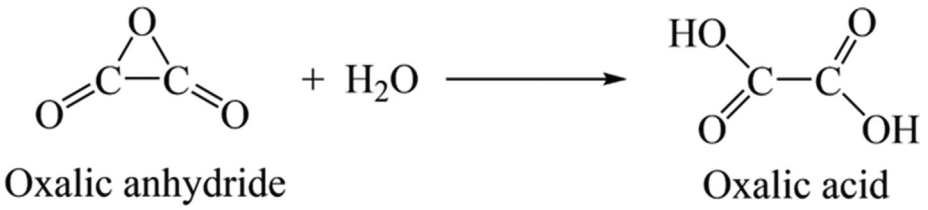

Fig. 8. Proposed hydrolysis reaction of oxalic anhydride forming oxalic acid.

Oxocarbon anions are cyclic aromatic structures that contain only oxygen and carbon atoms, such as deltate, squarate, croconate, and rhodizonate as can be seen in Fig. 7. Finally, C_2O is also an important ligand used in coordination chemistry (Frenking and Tonner, 2009).

The species C_2O_2, named ethenedione or carbon monoxide dimer is a fascinating species for a couple of reasons. It is a pretty simple molecule that, in principle, there is no reason not to exist. However, it was a challenging task to synthesize it (Trindle, 2003; Talbi and Chandler, 2000). This species is a dimer of carbon monoxide (Fig. 1d), and new oligomers of well-known molecules have been the subject of research for a long time. (Gambi et al. 2001; Groves and Lewars, 2000) Calculations indicate that its ground state should be a triplet, such as an oxygen molecule (Trindle, 2003; Talbi and Chandler, 2000) even that it is possible to infer a closed-shell Kekulé structure for this species.

The oxalic anhydride, C_2O_3, is a hypothetical organic species of particular interest because it can be seen as a precursor of a supposed prebiotic species (Lavado et al. 2019) which also highlight an astrobiological implication of the current work. It is important to mention that C_2O_3 could suffer a hydrolysis reaction to form oxalic acid, a well-known organic compound. Fig. 8 shows a proposed hydrolysis reaction of the oxalic anhydride to form oxalic acid. This reaction can easily occur since water molecules (and mainly water-rich ices) are ubiquitous structures found in the interstellar medium. (see also Perks & Liebman 2000, Talukdar 2020).

The quantification of chemical species not visible in the IR range may also contribute to a better estimate of the elemental abundance ratios in the solid-phase in astrophysical environments. For example, Sturm et al. (2022) used sub-millimeter observations with ALMA (Atacama Large Millimeter/Submillimeter Array) to show variations in the elemental abundances of C and H in the inner and outer part of protoplanetary disks, as well as, among different protostars. The same analysis is also possible for the solid-phase molecules using IR data of JWST. Although this quantification is mostly led by the number of chemical species observed in the spectrum, the IR inactive molecules such as O_2 or even much less abundant (e.g., C_2O and C_2O_3) may also be important to derive elemental abundances ratios between C and O in protoplanetary disks. The rate constants of these species derived with PROCODA and their use in gas-grain chemical models may be useful to derive reliable values in the context of molecular clouds and protostars.

Finally, we highlight that new insights on CO_2 ice chemistry will come out via observations with the James Webb Space Telescope (JWST), for example, with the abundance variation mapping of CO_2 ice in planet-forming regions. To understand the complexity of protostellar ices, chemical modeling such as the one employed by Ballering et al. (2021), which combines radiative transfer calculations with chemical data, is required. The results presented here, in special the determined ERC for reactions within the ice, the molecular abundances at CE phase, and the desorption yields, when employed in such models will help to put constraints on newly produced species (specially C_2O, C_2O_2, and C_2O_3) in the astronomical observations.

5. Conclusions

In this manuscript, we present an upgraded version of the PROCODA code (original code at Pilling et al 2022a) which describes the chemical evolution of ices processed

by ionizing radiation considering now an ordering hypothesis for the effective rate constants (ERCs) employing thermochemistry data (taken from literature) for the reactions within the groups of reactions. The current ordering hypothesis helps to identify the most important reactions within the reaction network and decreases the degeneracy of the solutions and enhancing the accuracy of the calculations (enhances the match between model and experimental data). Here, we described the chemical evolution of four experiments employing pure CO_2 ices processed by radiation: two ices bombarded by cosmic ray analogues (Pilling et al. 2010a; Mejía et al. 2015), one bombarded by 5 keV electrons (Bennett et al. 2004) and another irradiated by UV photons (Martín-Doménech et al. 2015). The main conclusions of this manuscript were:

i) The current results presented more accuracy when compared with previous calculations even understanding that solid-phase thermochemistry data is different from gas-phase and that some reaction might have activation barrier. This was observed in the value of summed chi-squared function (χ^2), which decreased by 22 % and 38 % in the current CR2 and UV model, respectively, compared with previous code version, as well as, in the CE criterion (slope similarity) which was closer to 100 % in the current version.
ii) The calculated average direct ERC were 6.4e-4, 7.5e-3, 2.1e-3 and 1.6e-3 s^{-1}, for the CR1, CR2, EL and UV models, respectively. For the bimolecular reactions the calculated average ERCs were 1.0e-26, 2.4e-25, 1.3e-25 and 1.0e-25 cm^3 $molecule^{-1}$ s^{-1}, for the CR1, CR2, EL and UV models, respectively. A comparison rates (only for CR2 and UV), between the average ERCs obtained here with the previous code version showed that the average direct and bimolecular reactions were roughly double the previous calculated value.
iii) Current calculated average intrinsic desorption ERCs were 8.4e-6, 2.9e-3, 1.2e-7, and 2.8e-4 s^{-1}, for the CR1, CR2, EL and UV models, respectively. These values (only for CR2 and UV) were 80 % higher than the ones obtained previously (see Pilling et al. 2022a). The desorption column density at the CE phase suggest that the experiments can be separated in two groups: group A – large desorption of parental species (the case of CR1 and EL models) and group B – large desorption of the daughter species CO (for CR2 and UV models).
iv) In the CE phase, the most abundant species were the CO_2, being considerably more abundant in the case of experiments employing electrons (92.6 %). The second most abundant species was the CO in most experiments, except in the case of CR2 model which was the oxygen atoms (29.1 %) a non-observed species in the ice. Additionally, the abundances of CO, O, C_2 and O_3, at the CE phase were considerably larger in the UV model than in the other models, which may help to constrain the main radiation field in the processing of ices present in different astrophysical regions.
v) The comparison between the upgraded version of the code with the previous one indicates that the ordering of ERCs by thermochemistry data in the models is much more important for the ices that are exposed to higher energy delivered as the case of CR2 model in respect with the UV model.

The upgraded PROCODA code is not only important to map the chemical evolution of simple ices under processing of radiation in the laboratory but also important to characterize the evolution of more complex ices (e.g·H_2O:CO:NH_3 ices, mixed ices containing water and organic species, etc.). This could allow the characterization of important organic species in the ices that were not detected by the experiments, with also important implications in the astrobiology field. We hope the current methodology helps to clarify the solid-state astrochemistry models of ices under the presence of radiation, as well as, helps to explain the observations of frozen and desorbed molecules in cold space environments.

Declaration of Competing Interest

The authors declare that they have no known competing financial interests or personal relationships that could have appeared to influence the work reported in this paper.

Acknowledgements

The authors thank the FVE/UNIVAP and the Brazilian research agencies CNPq (projects #304130/2012-5; #306145/2015-4; #302985/2018-2) and CAPES (grant PNPD/88887.368365/2019-0). The authors also thank prof. Galvão B. R. L. for the comments on the effective rate constants ordering hypothesis.

References

Almeida, G.C., Pilling, S., Andrade, D.P., Castro, N.L.S., Mendoza, E., Boechat-Roberty, H.M., Rocco, M.L.M., 2014. Photodesorption and photostability of acetone ices: Relevance to solid phase astrochemistry. The Journal of Physical Chemistry C 118 (12), 6193–6200. https://doi.org/10.1021/jp410745c.

Almeida, G.C., Pilling, S., de Barros, A.L.F., Da Costa, C.A.P., Pereira, R.C., Da Silveira, E.F., 2017. Processing of N2O ice by fast ions: implications on nitrogen chemistry in cold astrophysical environments. MNRAS 471 (2), 1330–1340. https://doi.org/10.1093/mnras/stx1438.

Alves, E., Franco, M.P., Pilling, S., Machado, F.B., Spada, R.F., 2021. The influence of the environment in chemical reactivity: the HCOOH formation from the H2O+ CO reaction. J. Mol. Model. 27 (9), 1–6. https://doi.org/10.1007/s00894-021-04872-4.

Andrade, D.P., de Barros, A.L., Pilling, S., Domaracka, A., Rothard, H., Boduch, P., da Silveira, E.F., 2013. Chemical reactions induced in frozen formic acid by heavy ion cosmic rays. MNRAS 430 (2), 787–796. https://doi.org/10.1093/mnras/sts408.

Atkins, P., Atkins, P.W., de Paula, J., 2014. Atkins' physical chemistry. Oxford University Press, UK.

Ballering, N.P., Cleeves, L.I., Anderson, D.E., 2021. Simulating Observations of Ices in Protoplanetary Disks. Astrophys J 920 (2), 115–127. https://doi.org/10.3847/1538-4357/ac17ed.

Baratta, G.A., Leto, G., Palumbo, M.E., 2002. A comparison of ion irradiation and UV photolysis of CH4 and CH3OH. A & A 384 (1), 343–349. https://doi.org/10.1051/0004-6361:20011835.

Baratta, G.A., Palumbo, M.E., 2017. The profile of the bending mode band in solid CO2. A & A 608, A81. https://doi.org/10.1051/0004-6361/201730945.

Bell, R. P., 1936. The theory of reactions involving proton transfers. In: Proceedings of the Royal Society of London. Series A-Mathematical and Physical Sciences, 154(882), 414-429. https://doi.org/10.1098/rspa.1936.0060.

Bennett, C.J., Jamieson, C., Mebel, A.M., Kaiser, R.I., 2004. Untangling the formation of the cyclic carbon trioxide isomer in low temperature carbon dioxide ices. PCCP 6 (4), 735–746. https://doi.org/10.1039/B315626P.

Bennett, C.J., Jamieson, C.S., Osamura, Y., Kaiser, R.I., 2006. Laboratory studies on the irradiation of methane in interstellar, cometary, and solar system ices. Astrophys J 653 (1), 792–811. https://doi.org/10.1086/508561.

Bennett, C.J., Jamieson, C.S., Kaiser, R.I., 2009. Mechanistical studies on the formation of carbon dioxide in extraterrestrial carbon monoxide ice analog samples. PCCP 11 (21), 4210–4218. https://doi.org/10.1039/B901220F.

Bennett, C.J., Jamieson, C.S., Kaiser, R.I., 2010. Mechanistical studies on the formation and destruction of carbon monoxide (CO), carbon dioxide (CO2), and carbon trioxide (CO3) in interstellar ice analog samples. PCCP 12 (16), 4032–4050. https://doi.org/10.1039/B917162B.

Bittner, D.M., Gope, K., Strasser, D., 2020. Time-resolved dissociative ionization and double photoionization of CO2. J. Chem. Phys. 153 (19), 194201–194300. https://doi.org/10.1063/5.0028812.

Boduch, P., Dartois, E., de Barros, A. L., da Silveira, E. F., Domaracka, A., Lv, X. Y., et al., 2015. Radiation effects in astrophysical ices. In Journal of Physics: Conference Series. Vol. 629, No. 1, 012008-012018. IOP Publishing. https://doi.org/10.1088/1742-6596/629/1/012008.

Boogert, A.A., Gerakines, P.A., Whittet, D.C., 2015. Observations of the icy universe. Ann. Rev. Astron. Astrophys. 53, 541–581. https://doi.org/10.1146/annurev-astro-082214-122348.

Bossa, J.B., Paardekooper, D.M., Isokoski, K., Linnartz, H., 2015. Methane ice photochemistry and kinetic study using laser desorption time-of-flight mass spectrometry at 20 K. PCCP 17 (26), 17346–17354. https://doi.org/10.1039/C5CP00578G.

Boyer, M.C., Rivas, N., Tran, A.A., Verish, C.A., Arumainayagam, C.R., 2016. The role of low-energy ($\leq$ 20 eV) electrons in astrochemistry. Surf. Sci. 652, 26–32 https://core.ac.uk/download/pdf/217023266.pdf.

Buratti, B.J., Cruikshank, D.P., Brown, R.H., Clark, R.N., Bauer, J.M., Jaumann, R., et al., 2005. Cassini visual and infrared mapping spectrometer observations of Iapetus: Detection of CO2. Astrophys J 622 (2), L149–L152. https://doi.org/10.1086/429800.

Cartwright, R.J., Emery, J.P., Rivkin, A.S., Trilling, D.E., Pinilla-Alonso, N., 2015. Distribution of CO2 ice on the large moons of Uranus and evidence for compositional stratification of their near-surfaces. Icarus 257, 428–456. https://doi.org/10.1016/j.icarus.2015.05.020.

Carvalho, G.A., Pilling, S., 2020a. X-ray photolysis of CH3COCH3 ice: implications for the radiation effects of compact objects towards astrophysical ices. MNRAS 498 (1), 689–701. https://doi.org/10.1093/mnras/staa2501.

Carvalho, G.A., Pilling, S., 2020b. Photolysis of CH3CN Ices by Soft X-rays: Implications for the Chemistry of Astrophysical Ices at the Surroundings of X-ray Sources. Chem. A Eur. J. 124 (41), 8574–8584. https://doi.org/10.1021/acs.jpca.0c06229.

Carvalho, G.A., Pilling, S., Galvão, B.R., 2022. Characterization of acetonitrile ice irradiated by X-rays employing the procoda code–I. Effective rate constants and abundances at chemical equilibrium. MNRAS 515 (3), 3760–3772. https://doi.org/10.1093/mnras/stac1965.

Chiar, J.E., Adamson, A.J., Kerr, T.H., Whittet, D.C.B., 1995. High-resolution studies of solid CO in the taurus dark cloud: Characterizing the ices in quiescent clouds. Astrophys J 455, 234 https://adsabs.harvard.edu/pdf/1995ApJ...455.234C.

Cottin, H., Moore, M.H., Bénilan, Y., 2003. Photodestruction of relevant interstellar molecules in ice mixtures. Astrophys J 590 (2), 874–881. https://doi.org/10.1086/375149.

De Barros, A.L.F., Da Silveira, E.F., Pilling, S., Domaracka, A., Rothard, H., Boduch, P., 2014. Processing of low carbon content interstellar ice analogues by cosmic rays: implications for the chemistry around oxygen-rich stars. MNRAS 438 (3), 2026–2035. https://doi.org/10.1093/mnras/stt2305.

de Souza Bonfim, V., de Castilho, R.B., Baptista, L., Pilling, S., 2017. SO3 formation from the X-ray photolysis of SO2 astrophysical ice analogues: FTIR spectroscopy and thermodynamic investigations. PCCP 19 (39), 26906–26917. https://doi.org/10.1039/C7CP03679E.

d'Hendecourt, L.B., Allamandola, L.J., Greenberg, J.M., 1985. Time dependent chemistry in dense molecular clouds. I-Grain surface reactions, gas/grain interactions and infrared spectroscopy. A & A 152, 130–150 https://adsabs.harvard.edu/full/1985A%26A...152.130D.

Ehrenfreund, P., Charnley, S.B., 2000. Organic Molecules In the Interstellar Medium, Comets, and Meteorites: A Voyage. Annu. Rev. Astron. Astrophys 38, 427–483. https://doi.org/10.1146/annurev.astro.38.1.427.

Ehrenfreund, P., Boogert, A.C.A., Gerakines, P.A., Tielens, A.G.G.M., Van Dishoeck, E.F., 1997. Infrared spectroscopy of interstellar apolar ice analogs. A & A 328, 649–669 https://adsabs.harvard.edu/full/1997A%26A...328.649E.

Evans, N.J., Dunham, M.M., Jørgensen, J.K., Enoch, M.L., Merín, B., Van Dishoeck, E.F., et al., 2009. The Spitzer c2d legacy results: star-formation rates and efficiencies; evolution and lifetimes. Astrophys. J. Suppl. Ser. 181 (2), 321–350. https://doi.org/10.1088/0067-0049/181/2/321.

Evans, M.G., Polanyi, M., 1936. Further considerations on the thermodynamics of chemical equilibria and reaction rates. Trans. Faraday Soc. 32, 1333–1360. https://doi.org/10.1039/TF9363201333.

Fillion, J.H., Fayolle, E.C., Michaut, X., et al., 2014. Wavelength resolved UV photodesorption and photochemistry of CO 2 ice. Faraday Discuss. 168, 533–552. https://doi.org/10.1039/C3FD00129F.

Flowers, P., Robinson, W.R., Langley, R., Theopold, K., 2015. Openstax Chemistry. Rice University, Houston, Texas, https://openstax.org/books/chemistry/pages/13-2-equilibrium-constants.

Fraser, H.J., McCoustra, M.R., Williams, D.A., 2002. Astrochemistry: The molecular universe. Astron. Geophys. 43 (2), 2–10. https://doi.org/10.1046/j.1468-4004.2002.43210.x.

Freitas, F.M., Pilling, S., 2020. Laboratory investigation of X-ray photolysis of methanol ice and its implication on astrophysical environments. Quim. Nova 43, 521–527 https://doi.org/10.21577/0100-4042.20170510.

Frenking, G., Tonner, R., 2009. Divalent carbon (0) compounds. Pure Appl. Chem. 81 (4), 597–614. https://doi.org/10.1351/PAC-CON-08-11-03.

Gambi, A., Giumanini, A.G., Strazzolini, P., 2001. Theoretical investigations on (CO) n (CO2) m cyclic cooligomers. J. Mol. Struct. (Thoechem) 536 (1), 9–16. https://doi.org/10.1016/S0166-1280(00)00601-1.

Garrod, R.T., Pauly, T., 2011. On the formation of CO2 and other interstellar ices. Astrophys J 735 (1), 15–33. https://doi.org/10.1088/0004-637X/735/1/15.

Gerakines, P.A., Schutte, W.A., Ehrenfreund, P., 1996. Ultraviolet processing of interstellar ice analogs. I. Pure ices. Astronomy and Astrophysics 312, 289–305 https://articles.adsabs.harvard.edu/full/1996A%26A...312.289G.

Gerakines, P.A., Whittet, D.C.B., Ehrenfreund, P., Boogert, A.C.A., Tielens, A.G.G.M., Schutte, W.A., et al., 1999. Observations of solid carbon dioxide in molecular clouds with the Infrared Space Observatory. Astrophys J 522 (1), 357–377. https://doi.org/10.1086/307611.

Gerakines, P.A., Moore, M.H., Hudson, R.L., 2004. Ultraviolet photolysis and proton irradiation of astrophysical ice analogs containing hydrogen cyanide. Icarus 170 (1), 202–213. https://doi.org/10.1016/j.icarus.2004.02.005.

Goumans, T.P.M., Uppal, M.A., Brown, W.A., 2008. Formation of CO2 on a carbonaceous surface: a quantum chemical study. MNRAS 384 (3), 1158–1164. https://doi.org/10.1111/j.1365-2966.2007.12788.x.

Gredel, R., Lepp, S., Dalgarno, A., Herbst, E., 1989. Cosmic-ray-induced photodissociation and photoionization rates of interstellar molecules. Astrophys J 347, 289–293 https://adsabs.harvard.edu/full/1989ApJ...347.289G.

Grim, R.J.A., d'Hendecourt, L.B., 1986. Time-dependent chemistry in dense molecular clouds. IV-Interstellar grain surface reactions inferred from a matrix isolation study. A & A 167, 161–165 https://articles.adsabs.harvard.edu/full/1986A%26A...167.161G.

Groves, C., Lewars, E., 2000. Dimers, trimers and oligomers of sulfur oxides: an ab initio and density functional study. J. Mol. Struct. (Thoechem) 530 (3), 265–279. https://doi.org/10.1016/S0166-1280(99)00384-X.

Hasegawa, T.I., Herbst, E., 1993. Three-Phase chemical models of dense interstellar clouds-Gas dust particle mantles and dust particle surfaces. MNRAS 263, 589–606. https://doi.org/10.1093/mnras/263.3.589.

Heyl, J., Viti, S., Holdship, J., Feeney, S.M., 2020. Exploiting network topology for accelerated Bayesian inference of grain surface reaction networks. Astrophys J 904 (2), 197–212. https://doi.org/10.3847/1538-4357/abbeed.

Holdship, J., Viti, S., Jiménez-Serra, I., Makrymallis, A., Priestley, F., 2017. UCLCHEM: a gas-grain chemical code for clouds, cores, and c-shocks. Astron. J. 154 (1) 38–48.https://doi.org/10.3847/1538-3881/aa773f.

Holdship, J., Jeffrey, N., Makrymallis, A., Viti, S., Yates, J., 2018. Bayesian Inference of the Rates of Surface Reactions in Icy Mantles. Astrophys J 866 (2), 116–125. https://doi.org/10.3847/1538-4357/aae1fa.

Huang, C.-H., Ciaravella, A., Cecchi-Pestellini, C., et al., 2020. Effects of 150–1000 eV Electron Impacts on Pure Carbon Monoxide Ices Using the Interstellar Energetic-Process System (IEPS). ApJ 889, 57 https://iopscience.iop.org/article/10.3847/1538-4357/ab5dbe/meta.

Hudson, R.L., Moore, M.H., 2001. Radiation chemical alterations in solar system ices: An overview. J. Geophys. Res. Planets 106 (E12), 33275–33284. https://doi.org/10.1029/2000JE001299.

Husain, D., & Young, A. N., 1975. Kinetic investigation of ground state carbon atoms, C (2 3 Pj). Journal of the Chemical Society, Faraday Transactions 2: Molecular and Chemical Physics, 71, 525-531. https://doi.org/10.1039/F29757100525.

Ioppolo, S., Van Boheemen, Y., Cuppen, H.M., Van Dishoeck, E.F., Linnartz, H., 2011. Surface formation of CO2 ice at low temperatures. MNRAS 413 (3), 2281–2287. https://doi.org/10.1111/j.1365-2966.2011.18306.x.

Jamieson, C.S., Mebel, A.M., Kaiser, R.I., 2006. Understanding the kinetics and dynamics of radiation-induced reaction pathways in carbon monoxide ice at 10 K. Astrophys. J. Suppl. Ser. 163 (1), 184–206. https://doi.org/10.1086/499245.

Jiménez-Escobar, A., Chen, Y.J., Ciaravella, A., Huang, C.H., Micela, G., Cecchi-Pestellini, C., 2016. X-ray irradiation of H2O+ CO ice mixtures with synchrotron light. Astrophys J 820 (1), 25–37. https://doi.org/10.3847/0004-637X/820/1/25.

Kaiser, R. I., & Roessler, K., 1998. Theoretical and laboratory studies on the interaction of cosmic-ray particles with interstellar ices. III. Suprathermal chemistry-induced formation of hydrocarbon molecules in solid methane (CH4), ethylene (C2H4), and acetylene (C2H2). The Astrophysical Journal, 503(2), 959-975. https://doi.org/10.1086/306001.

Kwok, S., 2016. Complex organics in space from Solar System to distant galaxies. Astron. Astrophys. Rev. 24 (1), 1–27 https://link.springer.com/article/10.1007/s00159-016-0093-y.

Lavado, N., de la Concepción, J.G., Gallego, M., Babiano, R., Cintas, P., 2019. From prebiotic chemistry to supramolecular oligomers: urea–glyoxal reactions. Org. Biomol. Chem. 17 (23), 5826–5838. https://doi.org/10.1039/C9OB01120J.

Linnartz H., Salama F. 2020, Laboratory Astrophysics: from Observations to Interpretations (Cambridge: Cambridge University Press) https://doi.org/10.1017/S1743921320000988.

Mallard, W. G., Westley, F., Herron, J. T., et al. 2004, NIST Chemical Kinetics Database Version 6.0, National Institute of Standards and Technology, Gaithersbyrg (MD). https://kinetics.nist.gov/.

Martín-Doménech, R., Manzano-Santamaría, J., Caro, G.M., Cruz-Díaz, G.A., Chen, Y.J., Herrero, V.J., Tanarro, I., 2015. UV photoprocessing of CO2 ice: a complete quantification of photochemistry and photon-induced desorption processes. A & A 584, A14–A25. https://doi.org/10.1051/0004-6361/201526003.

Mason, N.J., Nair, B., Jheeta, S., Szymańska, E., 2014. Electron induced chemistry: a new frontier in astrochemistry. Faraday Discuss. 168, 235–247. https://doi.org/10.1039/C4FD00004H.

McElroy, D., Walsh, C., Markwick, A.J., Cordiner, M.A., Smith, K., Millar, T.J., 2013. The UMIST database for astrochemistry 2012. A & A 550, A36–A49. https://doi.org/10.1051/0004-6361/201220465.

Meinert, C., Myrgorodska, I., De Marcellus, P., Buhse, T., Nahon, L., Hoffmann, S.V., et al., 2016. Ribose and related sugars from ultraviolet irradiation of interstellar ice analogs. Science 352 (6282), 208–212 https://www.science.org/doi/10.1126/science.aad8137.

Mejía, C., Bender, M., Severin, D., Trautmann, C., Boduch, P., Bordalo, V., et al., 2015. Radiolysis and sputtering of carbon dioxide ice induced by swift Ti, Ni, and Xe ions. Nucl. Instrum. Methods Phys. Res., Sect. B 365, 477–481. https://doi.org/10.1016/j.nimb.2015.09.039.

Mifsud, D.V., Kaňuchová, Z., Ioppolo, S., et al., 2022a. Mid-IR and VUV spectroscopic characterisation of thermally processed and electron irradiated CO2 astrophysical ice analogues. J. Mol. Spectrosc. 385. https://doi.org/10.1016/j.jms.2022.111599 111599.

Mifsud, D.V., Kaňuchová, Z., Ioppolo, et al., 2022b. Ozone production in electron irradiated CO 2: O 2 ices. PCCP 24 (30), 18169–18178. https://doi.org/10.1039/D2CP01535H.

Moll, N.G., Clutter, D.R., Thompson, W.E., 1966. Carbon trioxide: its production, infrared spectrum, and structure studied in a matrix of solid CO2. J. Chem. Phys. 45 (12), 4469–4481. https://doi.org/10.1063/1.1727526.

Moore, M. H., & Hudson, R. L., 1998. Infrared study of ion-irradiated water-ice mixtures with hydrocarbons relevant to comets. Icarus, 135 (2), 518-527.https://doi.org/10.1006/icar.1998.5996.

Muñoz Caro, G. M., Meierhenrich, U. J., Schutte, W. A., Barbier, B., Arcones Segovia, A., Rosenbauer, H., ... & Greenberg, J. M., 2002. Amino acids from ultraviolet irradiation of interstellar ice analogues. Nature, 416(6879), 403-406.https://www.nature.com/articles/416403a.

Öberg, K.I., Boogert, A.A., Pontoppidan, K.M., et al., 2011. The Spitzer ice legacy: Ice evolution from cores to protostars. Astrophys J 740 (2), 109–125. https://doi.org/10.1088/0004-637X/740/2/109.

Öberg, K. I. 2009, PhD thesis, Leiden Observatory, Faculty of Science, Leiden University.

Ohishi, M., Suzuki, H., Ishikawa, S.I., Yamada, C., Kanamori, H., Irvine, W.M., et al., 1991. Detection of a new carbon-chain molecule, CCO. Astrophys J 380, L39–L42 https://adsabs.harvard.edu/full/1991ApJ...380L.39O.

Okabe, H., 1978. Photochemistry of Small Molecules. Willey, New York.

Palumbo, M.E., 1997. Production of CO and CO2 after ion irradiation of ices. Adv. Space Res. 20 (8), 1637–1645. https://doi.org/10.1016/S0273-1177(97)00823-5.

Perks, H.M., Liebman, J.F., 2000. Paradigms and Paradoxes: Aspects of the Energetics of Carboxylic Acids and Their Anhydrides. Struct. Chem. 11 (4), 265–269. https://doi.org/10.1023/A:1009270411806.

Pilling, S., Bonfim, V.S., 2020. The influence of molecular vicinity (expressed in terms of dielectric constant) on the infrared spectra of

embedded species in ices and solid matrices. RSC Adv. 10 (9), 5328–5338. https://doi.org/10.1039/C9RA10136E.

Pilling, S., Andrade, D.P., Neto, A.C., Rittner, R., Naves de Brito, A., 2009. DNA nucleobase synthesis at Titan atmosphere analog by soft X-rays. Chem. A Eur. J. 113 (42), 11161–11166. https://doi.org/10.1021/jp902824v.

Pilling, S., Duarte, E.S., Domaracka, A., Rothard, H., Boduch, P., Da Silveira, E.F., 2010a. Radiolysis of H2O: CO2 ices by heavy energetic cosmic ray analogs. A & A 523, A77–A89. https://doi.org/10.1051/0004-6361/201015123.

Pilling, S., Duarte, E.S., Da Silveira, E.F., Balanzat, E., Rothard, H., Domaracka, A., Boduch, P., 2010b. Radiolysis of ammonia-containing ices by energetic, heavy, and highly charged ions inside dense astrophysical environments. A & A 509, A87–A97. https://doi.org/10.1051/0004-6361/200912274.

Pilling, S., Andrade, D.P.P., Do Nascimento, E.M., Marinho, R.R.T., Boechat-Roberty, H.M., De Coutinho, L.H., et al., 2011. Photostability of gas-and solid-phase biomolecules within dense molecular clouds due to soft X-rays. MNRAS 411 (4), 2214–2222. https://doi.org/10.1111/j.1365-2966.2010.17840.x.

Pilling, S., Bergantini, A., 2015. The effect of broadband soft X-rays in SO2-containing ices: implications on the photochemistry of ices toward young stellar objects. Astrophys J 811 (2), 151–173. https://doi.org/10.1088/0004-637X/811/2/151.

Pilling, S., Carvalho, G.A., Rocha, W.R., 2022a. Chemical Evolution of CO2 Ices under Processing by Ionizing Radiation: Characterization of Nonobserved Species and Chemical Equilibrium Phase with the Employment of PROCODA Code. Astrophys J 925 (2), 147–177. https://doi.org/10.3847/1538-4357/ac3d8a.

Pilling , S., Carvalho, G. A., de Abreu, H. A. , et al., 2022b, Understanding the molecular kinetics and the chemical equilibrium phase of frozen CO during bombardment by cosmic rays by employing the PROCODA code. Submitted to Astrophysical Journal.

Pilling, S., Mendes, L.A., Bordalo, V., Guaman, C.F., Ponciano, C.R., da Silveira, E.F., 2013. The influence of crystallinity degree on the glycine decomposition induced by 1 MeV proton bombardment in space analog conditions. Astrobiology 13 (1), 79–91. https://doi.org/10.1089/ast.2012.0877.

Pontoppidan, K.M., Fraser, H.J., Dartois, E., Thi, W.F., Van Dishoeck, E.F., Boogert, A.C.A., et al., 2003. A m VLT spectroscopic survey of embedded young low mass stars I-Structure of the CO ice. A & A 408 (3), 981–1007. https://doi.org/10.1051/0004-6361:20031030.

Pontoppidan, K.M., Boogert, A.C., Fraser, H.J., van Dishoeck, E.F., Blake, G.A., Lahuis, F., Salyk, C., 2008. The c2d Spitzer spectroscopic survey of ices around low-mass young stellar objects. II. CO2. Astrophys J 678 (2), 1005–1031. https://doi.org/10.1086/533431.

Portugal, W., Pilling, S., Boduch, P., Rothard, H., Andrade, D.P., 2014. Radiolysis of amino acids by heavy and energetic cosmic ray analogues in simulated space environments: α-glycine zwitterion form. MNRAS 441 (4), 3209–3225. https://doi.org/10.1093/mnras/stu656.

Poteet, C.A., Pontoppidan, K.M., Megeath, S.T., Watson, D.M., Isokoski, K., Bjorkman, J.E., et al., 2013. Anomalous CO2 Ice toward HOPS-68: A Tracer of Protostellar Feedback. Astrophys J 766 (2), 117–130. https://doi.org/10.1088/0004-637X/766/2/117.

Rachid, M.G., Faquine, K., Pilling, S., 2017. Destruction of C2H4O2 isomers in ice-phase by X-rays: Implication on the abundance of acetic acid and methyl formate in the interstellar medium. Planet. Space Sci. 149, 83–93. https://doi.org/10.1016/j.pss.2017.05.003.

Raut, U., Baragiola, R.A., 2011. Solid-state co oxidation by atomic o: A route to solid co2 synthesis in dense molecular clouds. The Astrophysical Journal Letters 737 (1), L14–L19. https://doi.org/10.1088/2041-8205/737/1/L14.

Rocha, W. R. M., Voitke, P., Pillind, S., et al., 2022, Simulation of CH3OH ice UV photolysis under laboratory Conditions, *Astronomy and Astrophysics,* submitted.

Ruaud, M., Wakelam, V., Hersant, F., 2016. Gas and grain chemical composition in cold cores as predicted by the Nautilus three-phase model. Monthly Notices of the Royal Astronomical Society 459 (4), 3756–3767. https://doi.org/10.1093/mnras/stw887.

Ruscic, B., Bross, D. H., 2020. Active Thermochemical Tables (ATcT) values based on ver. 1.122p of the Thermochemical Network 2020. https://atct.anl.gov/.

Ruscic, B., Pinzon, R. E., Von Laszewski, G., Kodeboyina, D., Burcat, A., Leahy, D., et al., 2005. Active Thermochemical Tables: thermochemistry for the 21st century. In *Journal of Physics: Conference Series.* 16, 561-570. IOP Publishing.https://doi.org/10.1088/1742-6596/16/1/078.

Ruscic, B., Pinzon, R.E., Morton, M.L., et al., 2004. Introduction to Active Thermochemical Tables: Several "Key" Enthalpies of Formation Revisited. J. Phys. Chem. A 108, 9979–9997. https://doi.org/10.1021/jp047912y.

se Graauw, T., Whittet, D. C. B., Gerakines, P. 2., Bauer, O. H., Beintema, D. A., Boogert, A. C. A., et al., 1996. SWS observations of solid CO_2_ in molecular clouds. Astronomy and astrophysics, 315, L345-L348. https://adsabs.harvard.edu/pdf/1996A%26A...315L.345D.

Seitz, G., Imming, P., 1992. Oxocarbons and pseudooxocarbons. Chem. Rev. 92 (6), 1227–1260. https://doi.org/10.1021/cr00014a004.

Seperuelo-Duarte, E., Boduch, P., Rothard, H., Been, T., Dartois, E., Farenzena, L.S., Da Silveira, E.F., 2009. Heavy ion irradiation of condensed CO: sputtering and molecule formation. A & A 502 (2), 599–603. https://doi.org/10.1051/0004-6361/200811359.

Seperuelo-Duarte, E., Domaracka, A., Boduch, P., Rothard, H., Dartois, E., Da Silveira, E.F., 2010. Laboratory simulation of heavy-ion cosmic-ray interaction with condensed CO. A & A 512, A71–A78. https://doi.org/10.1051/0004-6361/200912899.

Shingledecker, C.N., Vasyunin, A., Herbst, E., Caselli, P., 2019. On Simulating the Proton-irradiation of O2 and H2O Ices Using Astrochemical-type Models, with Implications for Bulk Reactivity. Astrophys J 876 (2), 140–150. https://doi.org/10.3847/1538-4357/ab16d5.

Sie, N.E., Caro, G.M., Huang, Z.H., et al., 2019. On the photodesorption of CO2 ice analogs: The formation of atomic C in the ice and the effect of the VUV emission spectrum. Astrophys J 874 (1), 35 https://iopscience.iop.org/article/10.3847/1538-4357/ab06be.

Silberberg, M., 2012. Principles of general chemistry. McGraw-Hill Education.

Sturm, J.A., McClure, M.K., Harsono, D., Facchini, S., Long, F., Kama, M., et al., 2022. Tracing pebble drift and trapping using radial carbon depletion profiles in protoplanetary disks. A & A 660, A126–A149. https://doi.org/10.1051/0004-6361/202141860.

Suhasaria, T., Baratta, G.A., Ioppolo, S., Zacharias, H., Palumbo, M.E., 2017. Solid CO2 in quiescent dense molecular clouds-Comparison between Spitzer and laboratory spectra. A & A 608, A12–A23. https://doi.org/10.1051/0004-6361/201730504.

Talbi, D., Chandler, G.S., 2000. Extensive ab Initio Study of the C2O2, C2S2, and C2OS Systems: Stabilities and Singlet− Triplet Energy Gaps. Chem. A Eur. J. 104 (24), 5872–5881. https://doi.org/10.1021/jp000732d.

Talukdar, R., 2020. Synthetically Important Ring-Opening Acylations of Alkoxybenzenes. Synthesis 52 (24), 3764–3780. https://doi.org/10.1055/s-0040-1707255.

Tielens, A.G.G.M., 2013. The molecular universe. Rev. Mod. Phys. 85 (3), 1021–1081. https://doi.org/10.1103/RevModPhys.85.1021.

Trindle, C., 2003. Spin preference in twenty-valence electron systems of form XCCY. Int. J. Quantum Chem 93 (4), 286–293. https://doi.org/10.1002/qua.10558.

Tsuge, M., Nguyen, T., Oba, Y., et al., 2020. UV-ray irradiation never causes amorphization of crystalline CO2: A transmission electron microscopy study. Chem. Phys. Lett. 760. https://doi.org/10.1016/j.cplett.2020.137999 137999.

van Dishoeck, E.F., 1988. Photodissociation and photoionization processes. In: Rate Coefficients in Astrochemistry. Springer, Dordrecht, pp. 49–72. https://doi.org/10.1007/978-94-009-3007-0_4.

van Dishoeck, E.F., 2014. Astrochemistry of dust, ice and gas: introduction and overview. Faraday Discuss. 168, 9–47. https://doi.org/10.1039/C4FD00140K.

van Dishoeck, E.F., Jonkheid, B., van Hemert, M.C., 2006. Photoprocesses in protoplanetary disks. Faraday Discuss. 133, 231–243. https://doi.org/10.1039/B517564J.

Vasconcelos, F.A., Pilling, S., Rocha, W.R.M., Rothard, H., Boduch, P., Ding, J.J., 2017a. Ion irradiation of pure and amorphous CH 4 ice relevant for astrophysical environments. PCCP 19 (20), 12845–12856. https://doi.org/10.1039/C7CP00883J.

Vasconcelos, F.A., Pilling, S., Rocha, W.R.M., Rothard, H., Boduch, P., 2017b. Radiolysis of N 2-rich astrophysical ice by swift oxygen ions: implication for space weathering of outer solar system bodies. PCCP 19 (35), 24154–24165. https://doi.org/10.1039/C7CP04408A.

Vasconcelos, F.A., Pilling, S., Rocha, W.R., Rothard, H., Boduch, P., 2017c. Energetic processing of N2: CH4 ices employing X-Rays and swift ions: implications for icy bodies in the outer solar system. Astrophys J 850 (2), 174–189. https://doi.org/10.3847/1538-4357/aa965f.

Wakelam, V., Smith, I.W.M., Herbst, E., Troe, J., Geppert, W., Linnartz, H., et al., 2010. Reaction networks for interstellar chemical modelling: improvements and challenges. Space Sci. Rev. 156 (1), 13–72. https://doi.org/10.1007/s11214-010-9712-5.